Characterisation of GaN using cathodoluminescence and photoluminescence spectroscopy

A thesis for the degree of
Master of Science

Presented to
Dublin City University

by

Brendan Ryan B.Sc.

Research Supervisor:
Professor M. O. Henry B.Sc. Ph.D.
August 2003

Declaration

I hereby certify that this material, which I now submit for assessment on the programme of study leading to the award of Master of Science is entirely my own work and has not been taken from the work of others save and to the extent that such work has been cited and acknowledged within the text of my work.

Signed: 

Identification number: 96041072

Date: 18 September 2003

Contents

Acknowledgements

I would like to thank my research supervisor Professor M. O. Henry for the giving me the chance to pursue research in his group. I thank him for his continued help, support, and encouragement throughout the project.

I would also like to thank Dr. Enda McGlynn for his support and advice throughout the course of the project.

I would like to thank Michael May for his initial training on the SEM and also for his continued support with maintenance of the facility and for addressing equipment based problems that arose during the course of the project. The assistance and support of both Michael and Dr. Lisa Looney was also greatly appreciated when changing the SEM stage for our low temperature work.

Thanks also to Des Lavelle, Patrick Wogan and Ray Murphy for addressing various problems that arose during the work. Also to James and Ger for assisting with the photoluminescence measurements.

For the ELO work I would like to thank Professor Patrick J. McNally and Donnacha Lowney for providing the samples for our experiments and for their contribution to the analysis and reviewing of the results.

Thanks also to Dr. Carol Trager-Cowan and other members of the Semiconductor Spectroscopy & Device Group at the University of Strathclyde, Glasgow for the courtesy shown to me during my visit and also for her advice on CL based matters. I would especially like to thank my parents and other family members who have supported me throughout my study.

Abstract

The electron beam used to generate SEM images often results in the emission of light (cathodoluminescence). If the luminescence is detected, a new and distinctive image of the sample is produced. This new CL-SEM image distinguishes regions of high and low luminescence efficiency. Cathodoluminescence spectroscopy is an irreplaceable research tool as it allows the researcher to obtain a correlation between structural and optical properties and well as providing high spatial resolution of the luminescence distribution in the sample.

In this study we apply CL-SEM to the study of GaN. Normal heteroepitaxial growth of GaN on substrates such as Al_2O_3 leads to a columnar material consisting of many hexagonal grains. The tilt and rotation of the grains result in a high dislocation density of the order of 10^{10} cm^{-2}. The effect of this high dislocation density on the luminescence efficiency was studied. In the Epitaxial Lateral Overgrowth (ELO) process, the material grows vertically through the etched windows in the SiO_2 mask and then laterally over the mask. This leads to a reduction in the dislocation density by three to four orders of magnitude. The results reported here confirm that the luminescence efficiency is substantially higher for ELO material.

We report also on photoluminescence measurements of a blue defect band in GaN which has received considerably less attention than the characteristic yellow band. The blue band appears for samples cooled in the dark, and it disappears under illumination at a rate that depends on temperature. We analyse the decrease in the blue luminescence and a corresponding increase of the yellow band as a function of time at a range of temperatures and suggest possible explanations for the complex nature of the metastability displayed by the defect responsible for the blue band.

List of Figures

List of Tables

1 Solid state theory

1.1 Material classification

An appreciation of the band theory of semiconductors may be gained by comparing them to other classes of materials with which we are more familiar, namely metals and insulators. Generally speaking metals have a high electrical conductivity. This feature is attributed to the high free electron concentration of approximately 10^{23} cm^{-3}. They are solids in which the application of an electric field causes an electric current to flow. In comparison, insulators possess a high resistance to electrical current. This is because of the lack of free carriers, since practically all the electrons in an insulator are bound to the crystal structure.

Semiconductors can change from insulating to metallic depending on the temperature and the impurity concentration. They can have a free carrier concentration from about 10^{9} to 10^{23} cm^{-3}. Adding small amounts of impurity atoms or changing the temperature of the material may cause this variation.

In a pure semiconductor the conductivity rises exponentially with temperature in the form of [Hummel 2001]:

$$\sigma_i = \sigma_{oi} \exp(-\frac{E_g}{2kT}) \qquad (1.1)$$

where σ_{oi} is a constant, E_g is the bandgap of the material, k is the Boltzmann constant, and T is the temperature.

At low temperature a small amount of impurities are required in order to achieve good conductivity. Depending on the type of impurities (donors or acceptors) added, the conductivity is due to either electrons or holes. The conductivity may be increased by exposure to light or to an electron beam.

While these effects are important, the single most important factor governing the properties of semiconductors is the energy gap, the origin of which is now discussed in some detail.

1.2 Energy band structure

The energy band structure may be understood by a consideration of the energy and momentum of a charge carrier in a solid. For an electron in free space the potential is zero and solving the Schrödinger equation shows that its energy is given by [Perkowitz 1993]:

$$E = \frac{p^2}{2m_o} \qquad (1.2)$$

where p is the momentum of the electron. In the band structure model the same equation applies, except that the rest mass m_o is replaced by the effective mass m^*. This may be smaller or larger than m_o.

For an electron in a crystal, the potential is periodic and a model is now considered which successfully incorporates this important factor.

1.2.1 Kronig – Penney model

This one-dimensional model proposed by R. de L. Kronig and W. G. Penney in 1930 can be used to illustrate the origin of energy bands in a crystal. The model consists of solving the Schrödinger equation for a periodic array of 1-D potential wells of width b, height V_o and separated by a distance a as shown in figure 1.1.

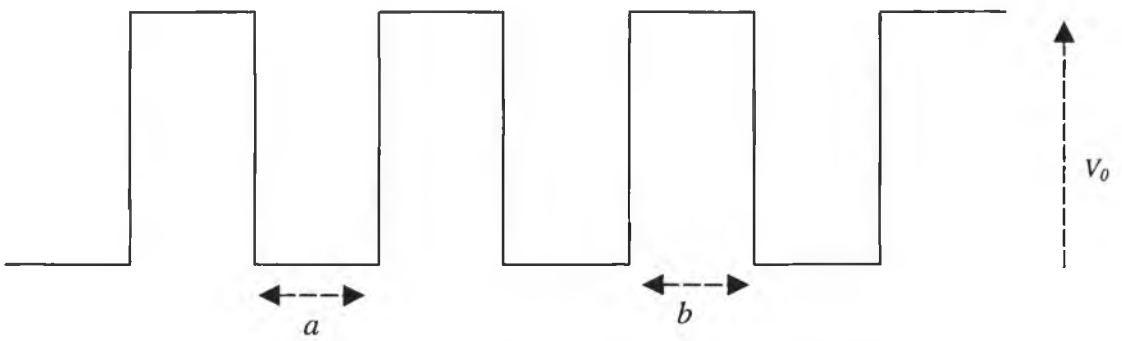

Figure 1.1: 1-D potential wells to illustrate the Kronig – Penney model

Subject to a chosen potential and certain boundary conditions ($b = 0$ & $V_o = \infty$ then a becomes the lattice constant) the equation that expresses the conditions for solutions to exist is given by [Rudden & Wilson 1993]:

$$\frac{w \sin \alpha a}{\alpha a} + \cos \alpha a = \cos ka \qquad (1.3)$$

where $\alpha^2 = \frac{8\pi^2 mE}{h^2}$ and k is the wavenumber, E is the electron kinetic energy and m the electron mass.

The quantity w is defined as the barrier strength. As a result if w is increased then the binding strength of a given electron to a particular potential well is also increased. When w decreases to zero, $\alpha = k$, and the energy spectrum is that of a free electron, that is continuous, with

$$E = \frac{h^2 k^2}{8\pi^2 m} \qquad (1.4)$$

The Kronig – Penney model predicts that discontinuities will occur on the otherwise parabolic E – k curve when:

$$k = \frac{n\pi}{a} \qquad n = 1,2,3 \ldots \qquad (1.5)$$

These k values define the Brillouin zones in the crystal. For instance values lying between $\frac{-\pi}{a}$ and $\frac{+\pi}{a}$ define the first Brillouin zone and values from $\frac{-\pi}{a}$ to $\frac{-2\pi}{a}$ or from $\frac{\pi}{a}$ to $\frac{2\pi}{a}$ define the second Brillouin zone as illustrated in figure 1.2.

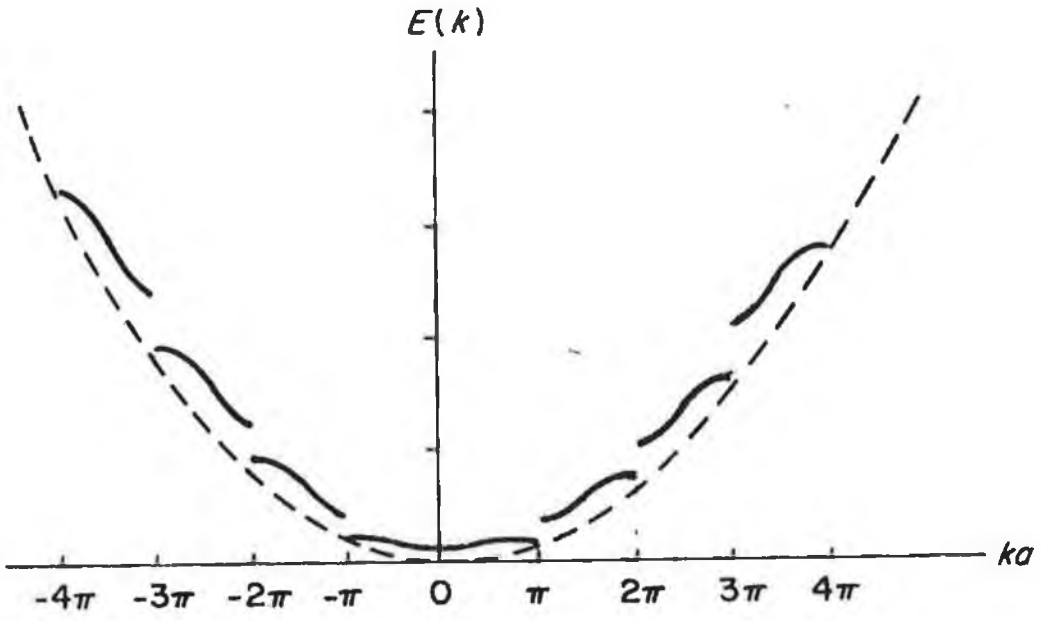

Figure 1.2: Plot of E - k for the Kronig – Penney model
[Rudden & Wilson 1993]

Therefore, since $k = \frac{2\pi}{\lambda}$ the expression $k = \frac{n\pi}{a}$ can be written as $n\lambda = 2a$. This represents Bragg reflection for normal incidence of the electron waves on areas separated by a the lattice constant (in the limit b =0).

So, within a band, energy is a periodic function of k. This is shown in figure 1.3.

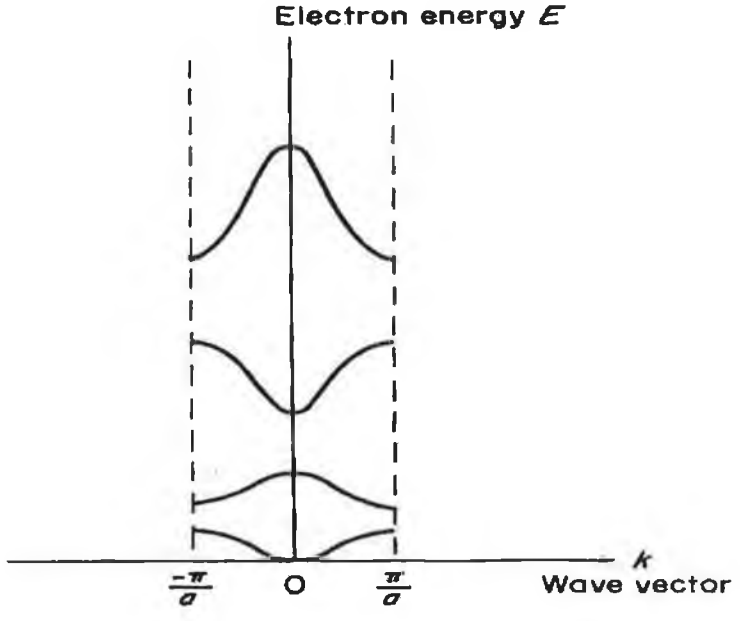

Figure 1.3: Reduced zone representation of E vs k curve
[Rudden & Wilson 1993]

1.3 Intrinsic and extrinsic luminescence

In semiconductors light is emitted as a result of electronic transitions between the conduction and valence bands of the material as well as transitions within the forbidden gap.

If a photon or electron of energy $> E_g$, where E_g is the bandgap of the material, is incident on a semiconductor electron hole (e-h) pairs are produced. This can lead to a number of transitions, which can be both intrinsic and extrinsic. The recombination processes shown in figure 1.4 will now be summarised, where E_x, E_D and E_A are the energy positions of the exciton, donor and acceptor levels respectively.

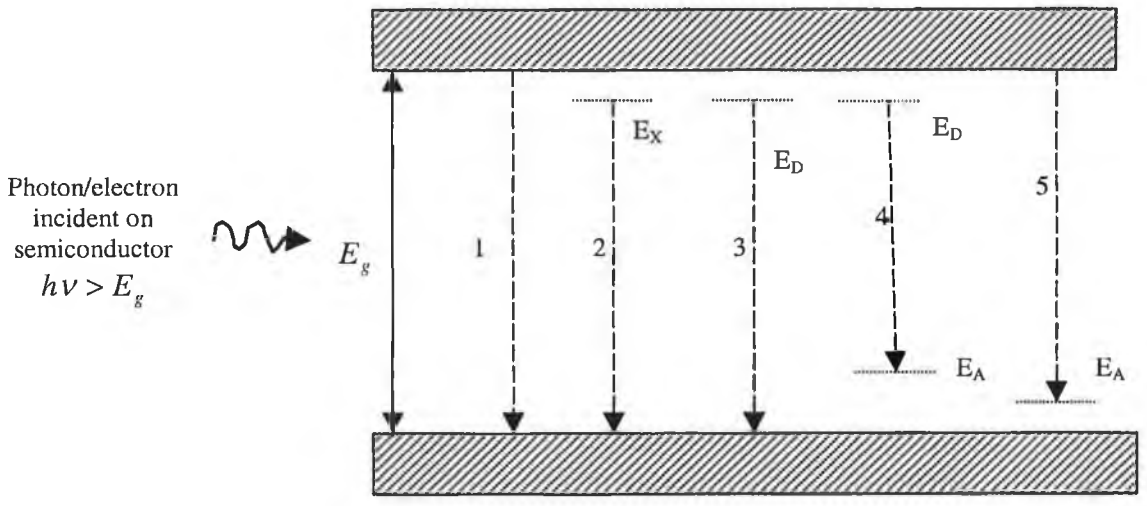

Figure 1.4: Schematic diagram of electronic transitions in a semiconductor

Process 1

Intrinsic transitions result in interband recombination of an electron in the conduction band with a hole in the valance band, resulting in the emission of a photon with energy approximately equal to E_g.

Process 2

Intrinsic transitions can also include free exciton decay. Excitons are produced in very pure semiconductors, usually at very low temperatures. They may be thought of

an electron and hole orbiting around their centre of mass. The magnitude of the exciton binding energy is given by [Bhattacharya 1994]:

$$|E_x| = \frac{-m_r^* q^4}{2(4\pi\varepsilon_r\varepsilon_0\hbar)} \cdot \frac{1}{n^2} \qquad n = 1,2,3\ldots \qquad (1.6)$$

Where m_r^* is the reduced effective mass, q is the electronic charge, ε_r is the relative permittivity, and ε_0 permittivity of free space.

The exciton decay is accompanied by the emission of a photon of energy [Omar 1975]:

$$h\nu = E_g - E_x \qquad (1.7)$$

Process 3

In this case recombination occurs between an electron in a shallow donor level and a hole in the valance band emitting a photon of energy $\leq E_g$.

Process 4

Transitions between an electron in a shallow donor to a hole in a deep acceptor level leads to the emission of photons, but in this case the energy is less than E_g.

Process 5

In this transition an electron in the conduction band recombines with a hole in a shallow acceptor level resulting in the emission of a photon of energy $\leq E_g$.

Note: Generally speaking extrinsic transitions may be more intense than intrinsic ones, as the emission of light is activated by the presence of impurities or native defects.

Bound excitons may be formed where impurities are present. Following their recombination, photons with energy [Petrov 1996]:

$$h\nu = E_g - E_x - E_b - mE_{ph} \qquad (1.8)$$

may be emitted, where E_b is the binding energy of the exciton to the impurity atom, m is the number of phonons emitted, and E_{ph} is the energy of the liberated phonons.

Luminescence from semiconductors is dominated by extrinsic recombination, but generally speaking it is only direct bandgap semiconductors that can act as efficient light emitters. The reasons for this shall now be discussed.

1.4 Direct and indirect transitions

During electronic transitions both energy and momentum must be conserved. If the filled states at the minimum of the conduction band and empty states at the maximum of the valance band occur at the same wavevector k then a direct transition may occur. Such materials are known as direct bandgap semiconductors, and they have many applications in the field of optoelectronics, such as laser diodes and light emitting diodes. Examples of direct bandgap materials include GaN, ZnO and GaAs.

If the filled states at the minimum of the conduction band and the empty states at the maximum of the valance band do not occur at the same wavevector, transitions will be indirect. These materials are called indirect bandgap semiconductors and recombination requires phonon participation. As a result the luminescence efficiency is far weaker for indirect bandgap semiconductors. Examples of such indirect bandgap materials include Si and GaP.

The direct and indirect recombination processes are illustrated in figure 1.5, where E_f and E_i are the energies of the final and initial states respectively.

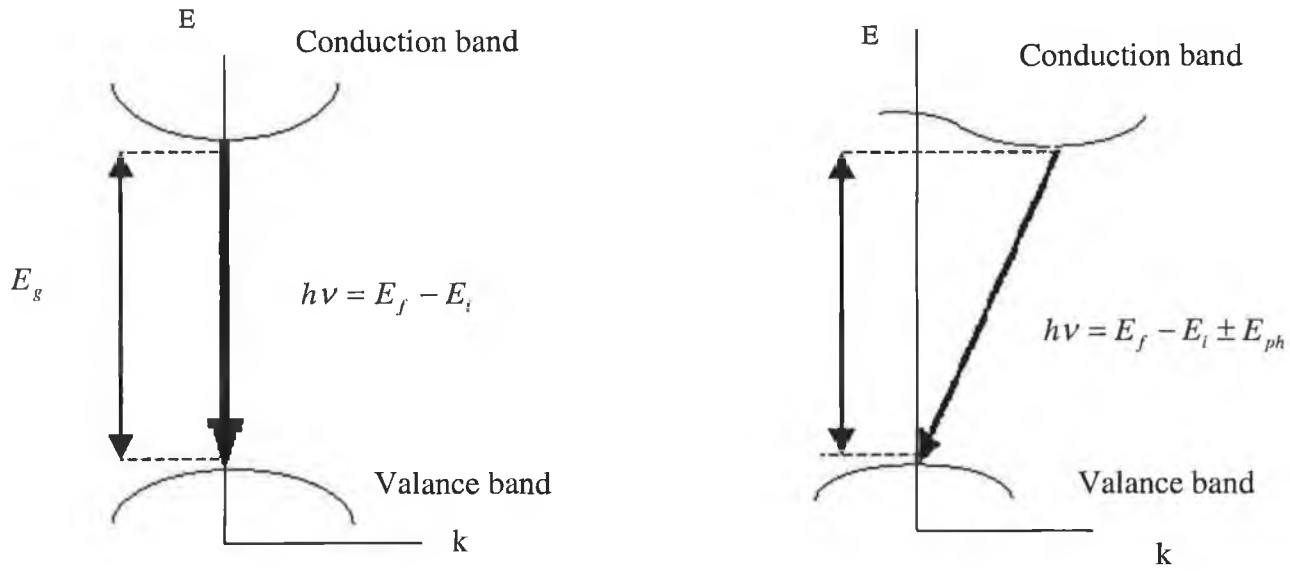

Figure 1.5: Interband recombination diagrams for a) direct and b) indirect bandgap semiconductors.

As discussed transitions can be either radiative or non-radiative. However phonon emission often accompanies many radiative transitions. The configuration coordinate model can be very useful in describing the phonon emission processes that accompany radiative transitions as well as describing the occurrence of broad bands in emission spectra.

1.5 Configuration coordinate model

The configuration coordinate diagram in figure 1.6 shows the energy of both the ground and excited state of an atom as a function of coordinate Q, relative to the equilibrium position in the crystal. At low temperatures the defect will be in its lowest state A. Absorption occurs to B, which is an excited state with the same atomic configuration. The phonon frequencies associated with the ground and excited states are assumed to be different, ω_o^g and ω_o^e respectively. The excited state may however have a minimum potential for a slightly different position of the atom. Therefore rapid non-radiative processes allow the system to relax to C with phonon participation. The mean number of phonons emitted is the Huang-Rhys factor

[Stoneham 1975]. When the electron returns to its ground state at D, a new atomic displacement is necessary in order for the system to relax to its lowest energy position A. The displacement from D to A also takes place with phonon participation. Generally LO-phonons are involved as they produce the strongest polarisation field, that is the strongest change per unit potential [Pankove 1971].

The configuration coordinate diagram proves very important when considering models for metastable defects as described in section 5.2. The shape of luminescence bands may also be understood using this model. The remainder of this section will include a brief description of this behaviour.

The shape of the luminescence band depends on $\hbar\omega_o^e$ and the Huang-Rhys factor S, which can be different for absorption and emission, S_{ab} and S_{em}. However, there is a relationship between these values [Reshchikov *et al.* 1999]:

$$\frac{S_{ab}}{S_{em}} = \frac{\hbar\omega_o^e}{\hbar\omega_o^g} \tag{1.9}$$

In the case of strong electron-phonon coupling ($S >> 1$), S represents the mean number of emitted phonons for each act of the photon absorption or emission. The larger the value of S, the wider the band and the less resolved are the transitions.

This will prove to be important in our discussion of the broad 2.9 eV luminescence band in GaN as will be discussed in section 5.3. The FWHM of the luminescence band, W, is a function of temperature and is given by [Reshchikov *et al.* 1999]:

$$W(T) = \left(\sqrt{8 \ln 2} \frac{S_{em} \hbar\omega_o^g}{\sqrt{S_{ab}}} \right) \sqrt{Coth\left(\frac{\hbar\omega_o^e}{2kT} \right)} \tag{1.10}$$

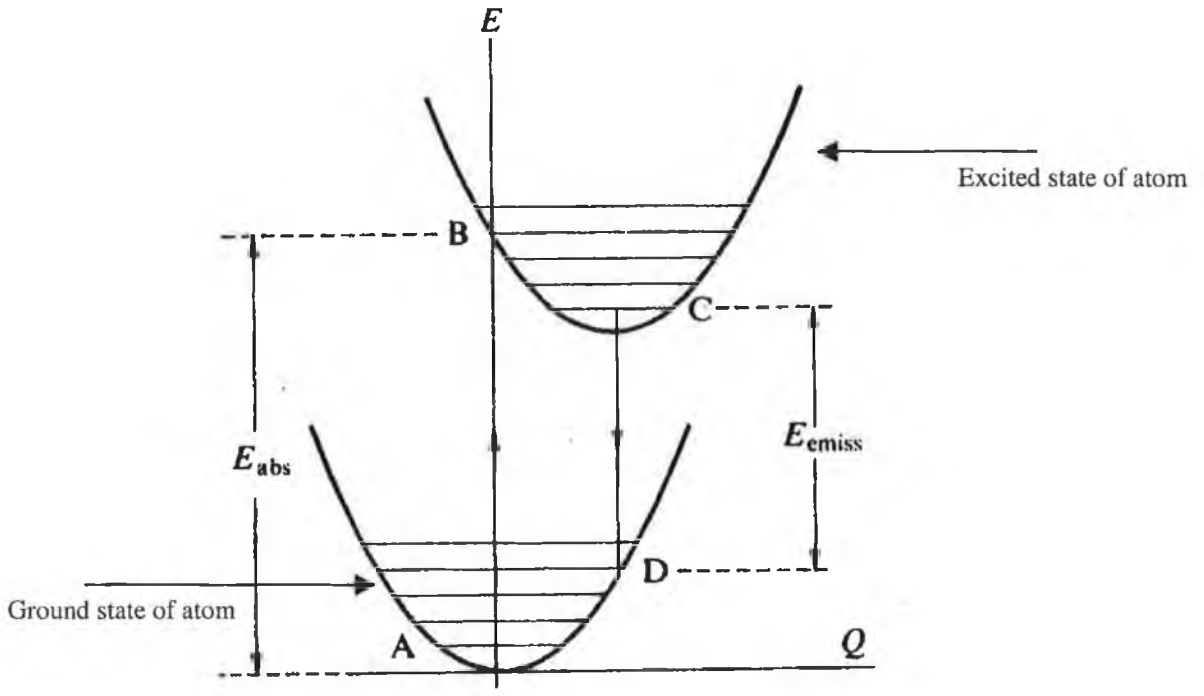

Figure 1.6: Configuration coordinate diagram
[Stoneham 1975]

1.6 Conclusion

Generally speaking the theory of semiconductors is very well developed, with excellent agreement with experiment for the principal spectroscopic techniques. This enables spectroscopic data to be analysed with considerable confidence for the usual types of luminescence (exciton, donor acceptor pairs, free to band transitions etc.) However, unusual phenomena continue to be reported for many semiconductors requiring a very thorough study and significant developments of the basic theory. Examples include the persistent photoconductivity (PPC) effect and related metastability in GaN which are currently the subject of many debates and the origin of which is relatively unknown.

2 Gallium Nitride

2.1 Introduction

The III-V semiconductors have recently been the subject of much research due to their wide range of applications. Gallium Nitride (GaN) is an important member of this family. It is a direct bandgap semiconductor and therefore can be used in many modern optoelectronic devices such as laser diodes (LD's) and light emitting diodes (LED's). It has a bandgap of ~ 3.4 eV at room temperature and for this reason it can be used for short wavelength applications [Orton *et al.* 1998].

GaN has good thermal conductivity and can be used in high temperature electronics, such as automobile engine sensors, as well as hostile environments, such as nuclear reactors and space applications [Koleske *et al.* 2000]. Table 2.1 outlines some of the properties of GaN [Pankove 1971].

Energy Gap (0 K) eV	Energy Gap (300 K) eV	Effective mass m^*_e	Effective mass m^*_h	Refractive index	Lattice constant Å	Electron mobility μ_e (cm^2/V. sec)
3.5	3.4	0.2	0.8	2.4	a = 3.18 c = 5.16	300

Table 2.1: Important material properties of GaN

As discussed in section 1.4 the radiative efficiency of indirect bandgap materials is low. As a result optoelectronic devices are made from direct gap compounds. Any direct gap material can in principle be used for the active regions in devices such as LED's and LD's, but in practice only a few are suitable. The main reasons for this are [Fox 2003]:

1. the size of the bandgap;
2. constraint relating to lattice matching;
3. the ease of p-type doping.

These important factors and how they specifically relate to GaN will be the subject of some discussion in this chapter. The relevance of the bandgap has however already been addressed in chapter 1.

2.2 Wurtzite structure of GaN

GaN crystallizes in both the cubic and hexagonal forms. For the purpose of this work the hexagonal Wurtzite structure was studied. The wurtzite unit cell is shown in figure 2.1 with the different lattice constants of GaN for each bond length.

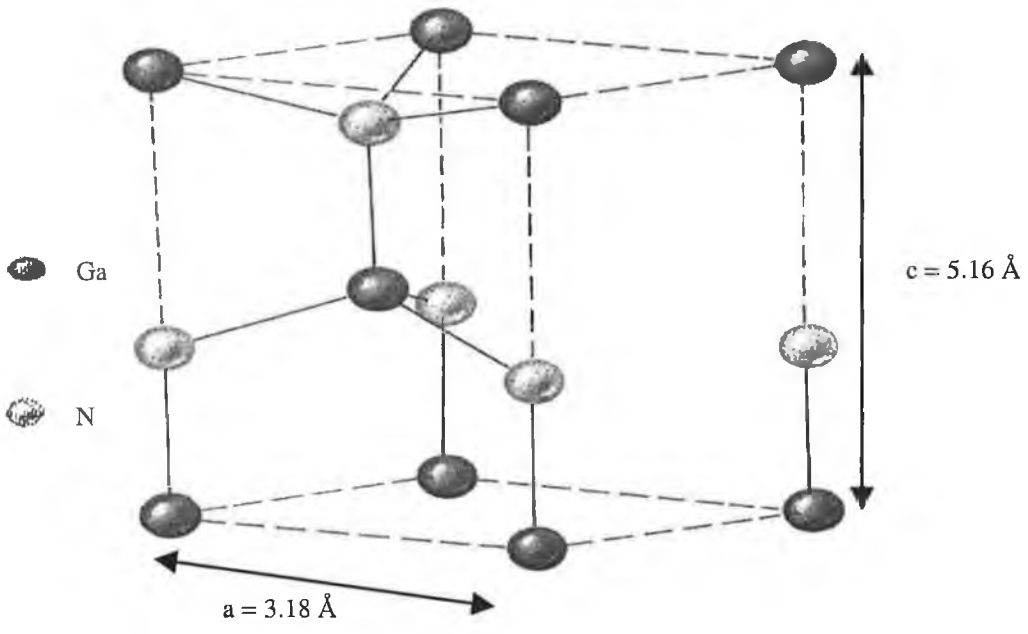

Figure 2.1: The unit structure cell for wurtzite GaN [Blakemore 1985]

Figure 2.2 shows the calculated band structure of GaN. Optical transitions occur at the point $\Gamma(k=0)$. Also, at $k=0$ the valance band is split into three bands. The relative positions of these bands are determined by a combination of spin-orbit splitting and axial crystal field strength. Each band gives rise to an exciton and each exciton gives rise to a hydrogenic series of energy levels [Orton *et al.* 1998].

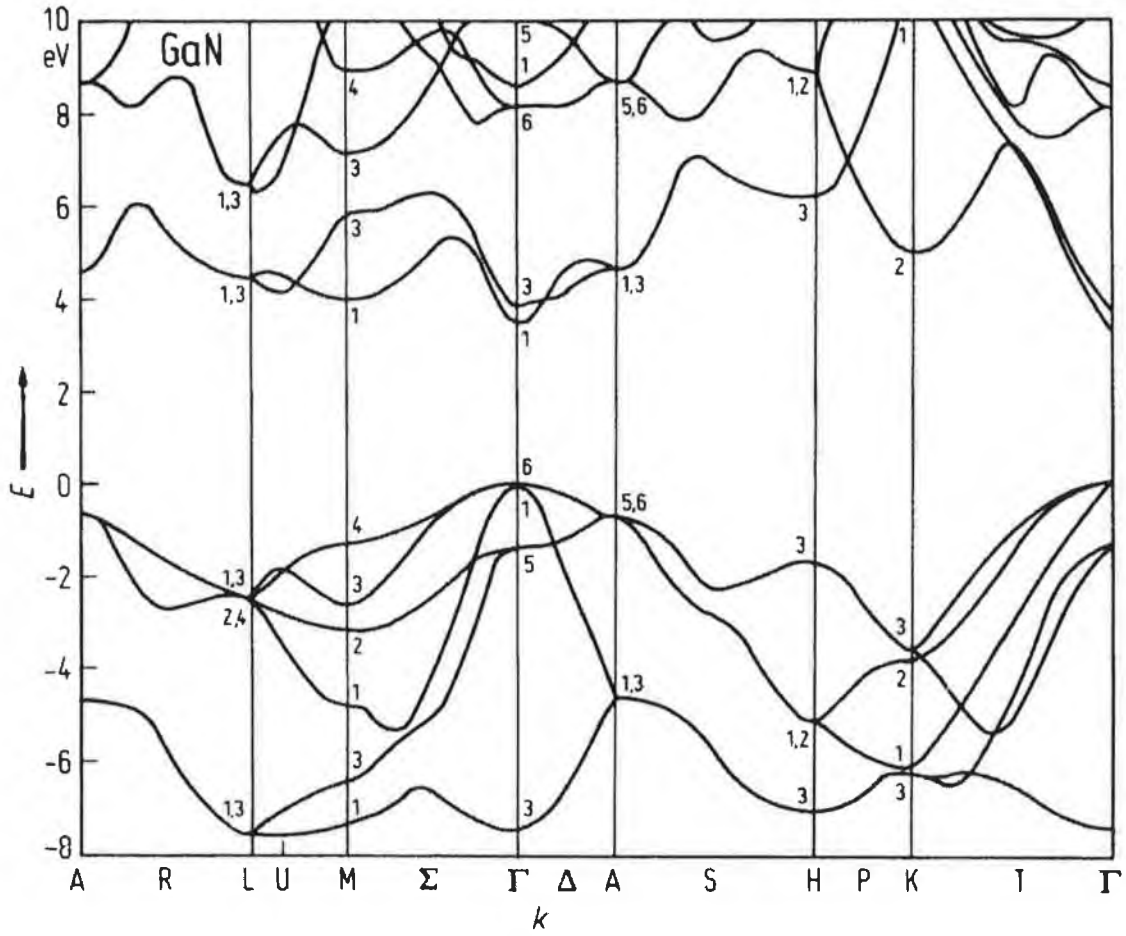

Figure 2.2: Calculated band structure for wurtzite GaN [Orton *et al.* 1998]

The following section addresses a vital issue that determines the materials which can be used to make good optoelectronic devices mentioned in the introduction to this chapter, namely lattice matching. Also discussed are measures to combat the constraints due to lattice matching by using growth techniques such as ELO growth.

2.3 Growth methods and lattice matching

Thin epitaxial layers are generally grown on top of crystal substrates. This is done for practical reasons. It has proven difficult to grow large crystals with sufficient purity to act as efficient light emitters. As a result thin layers of material are grown on substrates of poorer optical quality using techniques such as Hydride Vapour Phase Epitaxy (HVPE) [Kim *et al.* 1999] and Pulsed Laser Deposition (PLD) [Mah *et al.* 2001]. However where III-nitride epilayers are concerned Metal Organic Vapour

Phase Epitaxy (MOVPE) as well as Molecular Beam Epitaxy (MBE) are the more commonly used growth techniques [Jain *et al.* 2000].

The crystal growth conditions constrain the epitaxial layers to form the same crystal structure as the substrate. Thus the epitaxial layers will be highly strained unless the size of the lattice constant of both the substrate and epilayer are roughly the same. Figure 2.3 shows a plot of the bandgap (eV) versus the lattice constant (Å) for a number of semiconductors.

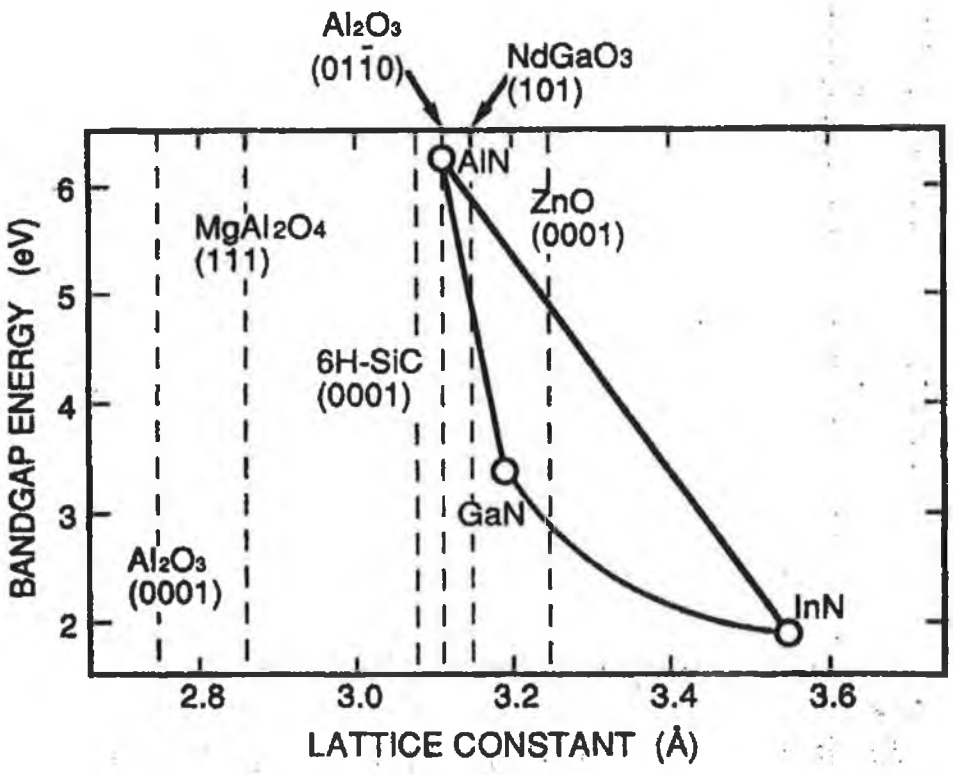

Figure 2.3: Plot of bandgap versus lattice constant of various semiconductors [Matsuoka 1997]

The top of the figure shows the lattice constants of the more commonly used substrates for both hexagonal and cubic materials. As can be seen the more suitable substrates for growing GaN are SiC and Sapphire. The following subsections will examine the merits and demerits of GaN grown on sapphire and will also introduce a far superior technique for growing GaN.

2.3.1 Sapphire substrates

Sapphire is the most extensively used substrate for growing GaN epilayers. This is due to the fact that large area good quality wafers can be produced at low cost. It is transparent and stable at high temperatures and the technology of the growth is mature [Jain *et al.* 2000].

However a lattice mismatch exists between the epilayer and the substrate. This is due to the difference in lattice constants of the GaN and Al_2O_3 and also to the difference in the thermal expansion coefficients of the two materials. These parameters are summarized in table 2.2.

	GaN	**Al_2O_3**
Lattice constant (c) Å	3.186	2.747
Thermal expansion coefficient $*10^{-6}K^{-1}$	5.59	7.5

Table 2.2: Constants for GaN and Al_2O_3 [Bell *et al.* 2001]

Although it is clear that the lattice constants of the two materials are different an epitaxial layer can be grown on a substrate of slightly different lattice constant provided the thickness of the layer is sufficiently small. If the thickness h of the layer is smaller than a certain critical thickness h_c, the misfit between the layer and substrate is accommodated by a tetragonal compression of the layer as seen in figure 2.4 (a) [Jain *et al.* 2000]. The critical thickness h_c is given by [Jain *et al.* 2000]:

$$h_c = \frac{b^2(1-\nu\cos^2\beta)}{8\pi f_m(1+\nu)b_1}\ln\frac{\rho_c h_c}{q} \qquad (2.1)$$

where b is the Burgers vector, $b_1 = b\cos\beta$, where β is the angle between the dislocation line and its Burgers vector, q is the core parameter and is assumed to be equal to b, ν is the Poisson's ratio, and ρ_c is the core energy parameter.

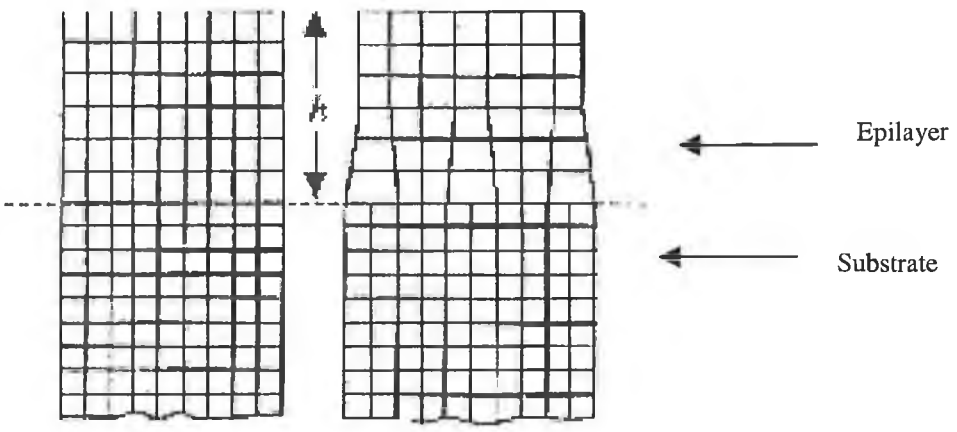

Figure 2.4: Structure of epilayer under biaxial compression a) Pseudomorphic and b) relaxed (with misfit dislocations) [Jain *et al.* 2000]

If on the other hand the lattice constant of the epilayer is smaller than that of the substrate the strain is tensile.

When $h > h_c$, misfit strain begins to relax by the introduction of misfit dislocations, as shown in figure 2.4 (b).

The lattice mismatch misfit parameter f_m [Jain *et al.* 2000] and thermal strain ε_T [Bell *et al.* 2001] may be calculated from:

$$f_m = \frac{a_2 - a_1}{a_1} \qquad (2.2)$$

$$\varepsilon_T = \Delta\alpha\Delta T \qquad (2.3)$$

Where a_1 is the lattice constant of sapphire, a_2 is the lattice constant of GaN, $\Delta\alpha$ is the difference in thermal expansion coefficients, and ΔT is the increase in temperature. In the case of GaN the misfit parameter is ~ 15 %.

The crystal orientations of GaN grown on c-plane [0001] sapphire are parallel, but the unit cell of GaN is rotated by 30^0 about the c-axis with respect to the sapphire unit cell [Hersee *et al.* 1997] as seen in figure 2.5.

This lattice misfit parameter along with the unit cell rotation can have a detrimental effect on the luminescence properties of GaN based devices. However in recent years a number of growth techniques such as pendeoepitaxy, where trenches are etched in a GaN layer and growth conditions are adjusted so that subsequent GaN growth occurs

from the trench sidewalls, and epitaxial lateral overgrowth (ELO) have made considerable advances in producing better quality material.

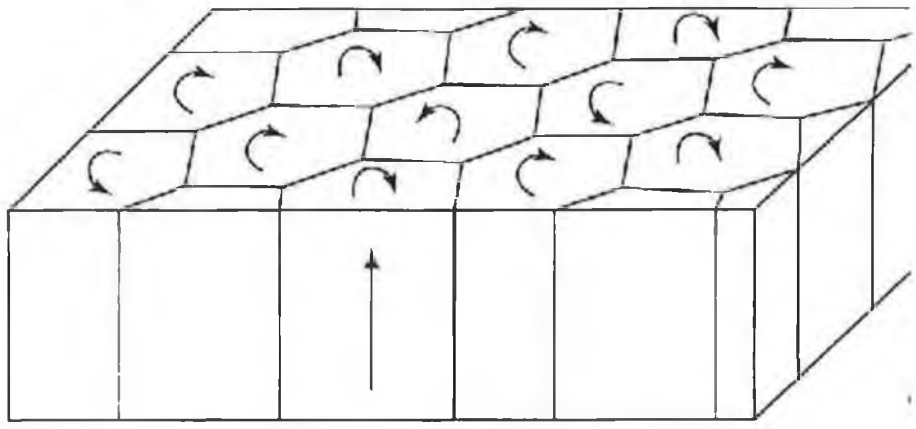

Figure 2.5: Rotation of GaN with respect to Al_2O_3
[Yu *et al.* 1998]

2.3.2 Epitaxial lateral overgrowth substrates

As discussed previously, epitaxial growth of GaN on sapphire leads to a columnar material consisting of hexagonal grains, which have a tilt and rotation within the film. As seen this gives rise to a very large dislocation density of the order of 10^{10} per cm^2 [Yu *et al.* 1998], [Johnson *et al.* 1999]. The Epitaxial Lateral Overgrowth process is now described for GaN, which is reported to reduce the dislocation density by 3-4 orders of magnitude [Amokrane *et al.* 2000]. This process is illustrated in figure 2.6.

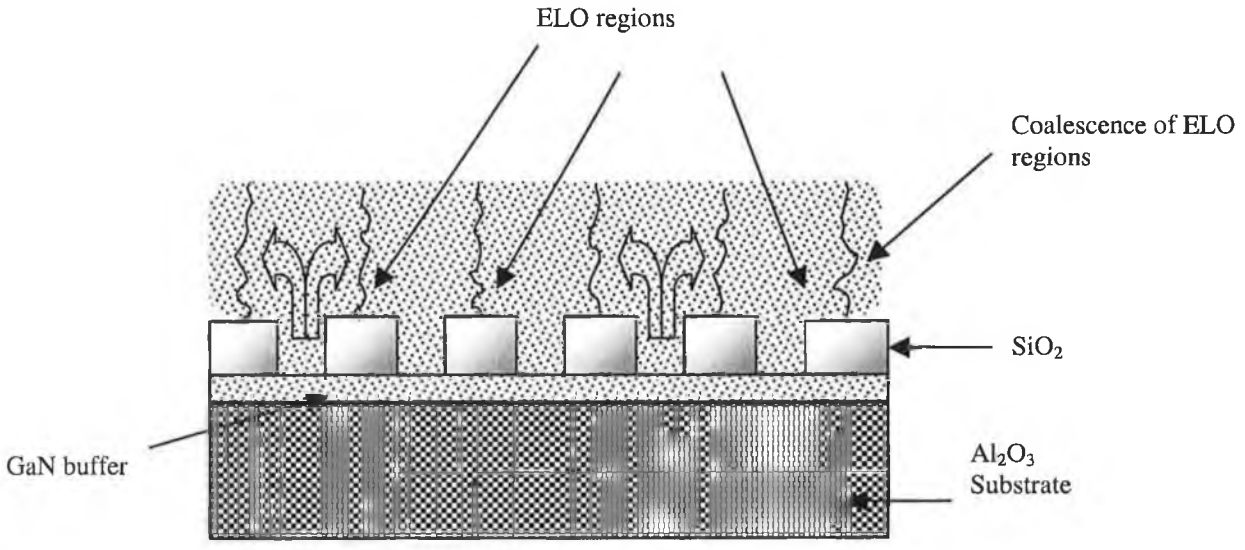

Figure 2.6: Illustration of ELO growth process

In ELO growth openings in a SiO_2 mask facilitate growth of GaN from the underlying seed material. Initially the growth proceeds vertically through the window opening and then laterally over the mask. The dislocation density in the resulting epilayer, in areas marked 'ELO regions' in figure 2.6 are significantly smaller due to vertically blocking of some of the propagating dislocations and a redirection of others. As a result the GaN directly over the SiO_2 should be of much higher quality than the material that grows vertically through the windows. This fact can be verified by using suitable sensitive spectroscopy techniques such as cathodoluminescence.

The ELO growth method has allowed great advancements to be made in the field of optoelectronics. It has allowed companies such as Nichia Chemicals to design and build laser diodes on the low-density dislocation ELO stripes, with a lifetime exceeding

1150 hours [Nakamura *et al.* 1998]. However the development of the III-V semiconductors took some time, due mainly to doping problems. This is the third important point mentioned in the introduction which determines the development of optoelectronic devices. This serious problem and efforts that were taken to solve the problem will now be the subject of a short discussion in the case for GaN.

2.4 N and P – type GaN

Generally speaking GaN is n-type material. One of the reasons for this is that oxygen is very abundant as an adsorbate on the walls of the reactor and often as H_2O in the ammonia used to synthesize the nitride [Seifert *et al.* 1983]. Hence oxygen is often introduced to the material unintentionally and the concentration is difficult to control. As a result researchers tend to use Si as a donor, which can be added controllably during the growth of GaN [Pankove 1999]. It should be noted that Si can act as an acceptor if it replaces a N rather than a Ga atom. However since the bonding of Si to Ga is less probable it is normally used as a donor.

Interestingly the development of blue nitrides has taken much time. It has been known for some time that the nitrides could potentially make good blue emitters. The reason for the slow progress is due to the lack of suitable p-type dopants. This problem has slowed the development of many wide bandgap materials. For instance the wide bandgap materials ZnSe and CdSe should in principle make good emitters, but their progress has been hampered due to doping problems [Fox 2003].

The reason why p-type doping is very difficult in these materials is due to the fact that wide bandgap materials have very deep acceptor levels. One of these deep acceptor levels is the well known Ga vacancy V_{Ga}^{3-}, which has recently been the subject of much research in its relationship with the 2.9 and 2.2 eV defect bands in GaN. The energy of the acceptor levels are given by [Fox 2003]:

$$E_n^A = -\frac{m_h^*}{m_o}\frac{I}{\varepsilon_r^2}\frac{R_H}{n^2} \qquad (2.4)$$

where m_h^* is the hole effective mass, m_o is the free electron mass, ε_r is the dielectric constant for the material and R_H is the Rydberg constant. Since the hole effective mass is quite large, as seen in table 2.1 and ε_r is relatively small, the acceptor energy E_n^A is large, resulting in deep acceptor levels. As a result less holes can be excited into the valance band following excitation by passing a current through the device and therefore good p-type conductivity is difficult to achieve. Since there is a low

hole density in n-type material there is high resistivity when a current flows through the device. This results in ohmic heating and therefore rendering devices useless.

Many impurities were tried as potential acceptors [Pankove 1999]. Magnesium was tried but the Mg atoms produce an acceptor level 0.3 eV above the valance band making it too deep for conducting p-type material. Carbon which was very successful in making conducting p-type GaAs is also a deep level in GaN [Fox 2003]. As a result many research groups were discouraged from searching for suitable p-type dopants.

In 1988 an accidental discovery was made [Akasaki *et al.* 1988]. Cathodoluminescence was being performed on a GaN:Mg sample. The longer the beam in the scanning electron microscope was scanned the brighter the blue luminescence appeared to be. This was explained by the fact that hydrogen was passivating a shallow acceptor level of Mg and the electron beam provided enough energy to break away the H and free the shallow acceptor [Van Vechten *et al.* 1992].

Later experiments showed that during thermal annealing above 700^0 C the passivating H was being removed from Mg resulting in p-type GaN. This is illustrated in figure 2.7 [Nakamura *et al.* 1992].

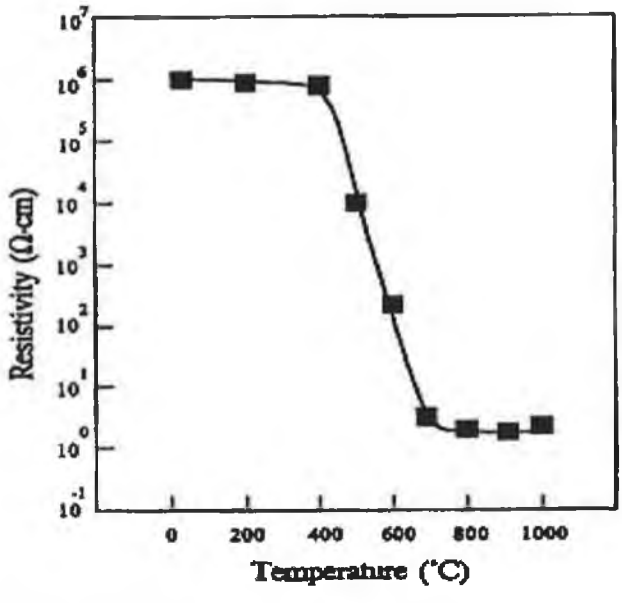

Figure 2.7: Resistivity of GaN:Mg after annealing at different temperatures [Nakamura *et al.* 1992]

The figure shows a very low resistivity value at ~ 700^0 C, which was direct evidence for conducting p-type material.

2.5 Conclusion

This chapter discussed many of the important material parameters of GaN and has suggested methods of overcoming the hazards of lattice mismatched materials by utilisation of the ELO process. It has also discussed how earlier problems in making good quality devices were overcome. For this reason much research, especially in the last 10 years, has been concentrated on the III-V semiconductors and in general wide bandgap materials.

The results section of this work will show in detail how the ELO process has contributed to the development of GaN based material and will also discuss the physics behind the defect bands and their interrelationship.

The intrinsic deep acceptor V_{Ga}^{3-} in GaN was introduced and the reasons behind many acceptors being deep levels in wide bandgap materials were also addressed. The nature and understanding of this deep level defect is of utmost importance in discussing the origin of the defect bands as will be seen in chapters 4 and 5.

3 Characterisation techniques

Luminescence spectroscopy is a very sensitive tool for investigating intrinsic and extrinsic transitions in semiconductors. Vital information may be obtained on the optical quality of materials. Information such as bandedge wavelength, exciton peaks, and below bandgap defect levels may be acquired from luminescence spectra. Some of the more important techniques currently used include photoluminescence and cathodoluminescence spectroscopy. This chapter shall facilitate a description of both photoluminescence and cathodoluminescence spectroscopy and detail the experimental setup in each case.

3.1 Photoluminescence spectroscopy

Photoluminescence spectroscopy is a contactless, nondestructive method of probing the electronic structure of materials. Light is directed onto a sample, where it is absorbed and imparts excess energy into the material in a process called photoexcitation. One way this excess energy can be dissipated by the sample is through the emission of light, or luminescence. In the case of photoexcitation, this luminescence is called photoluminescence. The intensity and spectral content of this photoluminescence is a direct measure of various important material properties. Specifically, photoexcitation causes electrons within the material to move into permissible excited states. When these electrons return to their equilibrium states, the excess energy is released and may include the emission of light (a radiative process) or may not (a nonradiative process). The energy of the emitted light is related to the difference in energy levels between the two electron states involved in the transition, that is, between the excited state and the equilibrium state. The quantity of the emitted light is related to the relative contribution of the radiative process. A very useful form of photoluminescence spectroscopy is Fourier Transform spectroscopy. Some of the main features of this technique shall now be the subject of a short description [Chamberlain 1979].

3.1.1 Fourier Transform spectroscopy

Fourier transform spectroscopy is based on the two beam Michelson interferometer as shown in figure 3.1. As mirror A moves the optical path length traveled by the light in arm A changes with respect to the optical path traveled by the light in arm B. When the two beams recombine at the beam splitter there will be a phase difference between them. Changing the position of mirror A alters this phase. The signal intensity at the detector will depend on the relative phase of the two beams, that is whether they interfere constructively or destructively.

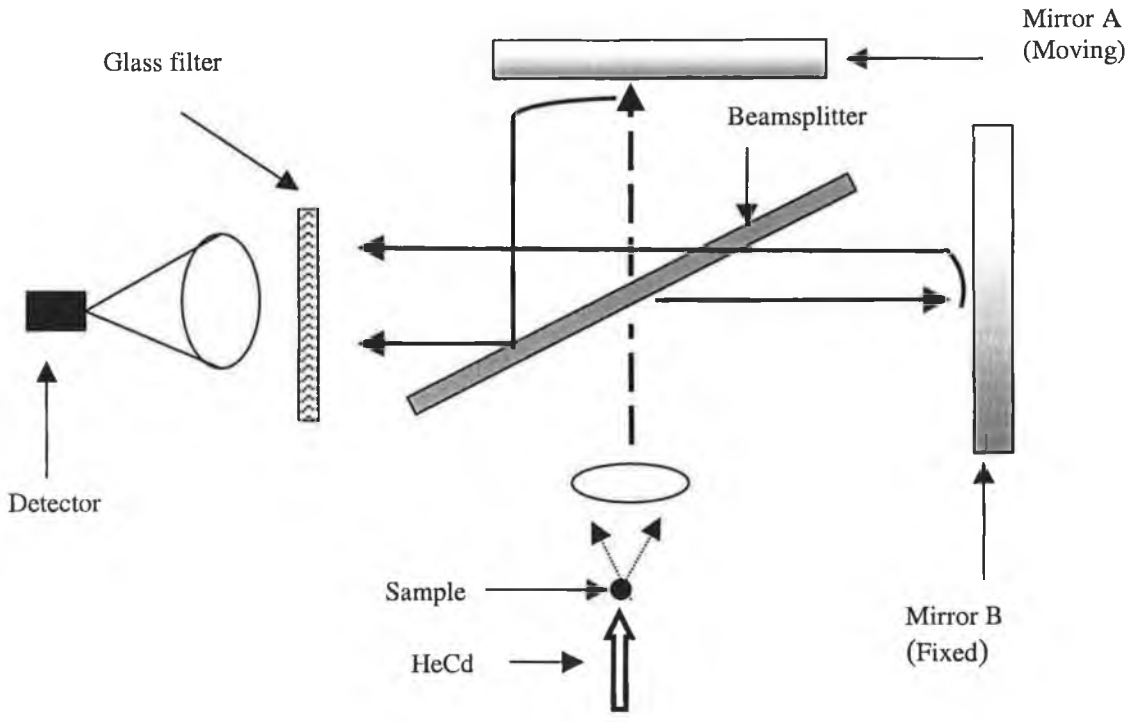

Figure 3.1: Michelson interferometer used in Fourier Transform spectroscopy

The electric fields of the two light waves as a function of position x and time t are described by:

$$E_1 = E_0 \sin(kx - \omega t) \qquad (3.1)$$

$$E_2 = E_0 \sin(kx - \omega t + \phi) \qquad (3.2)$$

where k is the wavenumber, ω is the angular frequency and ϕ is the relative phase difference of the two waves, which is dependent on the mirror position.

When mirror A moves a distance d relative to mirror B, the light in A must travel an extra distance $2d$ with respect to the light in path B.

The number of extra wavelengths travelled by A is given by:

$$N = \frac{2d}{\lambda} \tag{3.3}$$

and the corresponding phase angle ϕ is given by:

$$\phi = \frac{2\pi 2d}{\lambda} = 2kd \tag{3.4}$$

Adding E_1 and E_2 the resultant light wave electric field E_T is given by:

$$E_T = E_1 + E_2 = E_0[\sin(kx - \omega t) + \sin(kx - \omega t + \phi)] \tag{3.5}$$

The intensity at the detector is obtained by squaring E_T.

$$I(d) = E_T^2 = E_o^2 + E_o^2 \cos kd \tag{3.6}$$

As can be seen from equation 3.6 the detector intensity varies sinusoidally with mirror position.

The plot of detector intensity versus mirror position is called an interferogram an example of which is shown in figure 3.2. From the interferogram a Fourier transform calculation is performed resulting in a spectrum of intensity (I) versus wavelength (λ).

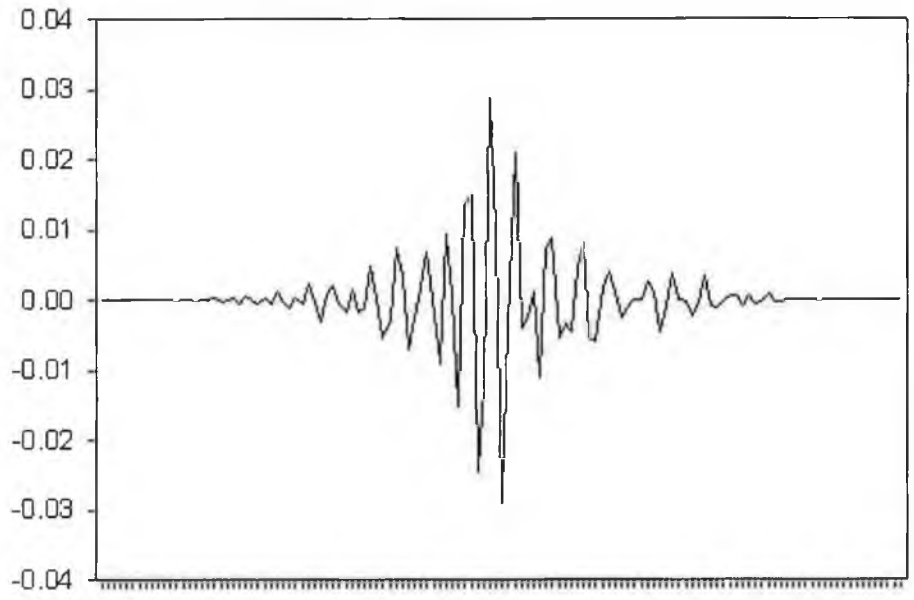

Figure 3.2: Interferogram used in Fourier Transform spectroscopy

3.1.2 Fourier Transform apparatus

The photoluminescence experimental set-up consists of the 325 nm line of a continuous wave HeCd laser (output ~ 20 mW unfocussed on the sample) providing PL excitation. The emission from the sample was analyzed using a Bomem DA8 Fourier-Transform spectrometer fitted with a Hamamatsu R1913 PM-tube. A glass filter sensitive to the spectral range 300-600 nm was inserted in front of the PM-tube detector to analyse the wavelengths of interest for this work.

Samples can be studied at temperatures between 15 K and 300 K using a Janis CCS-500 closed-cycle cryostat. The spectrometer was operated in phase acquisition mode, which acquires a spectrum over the entire wavelength range in order to calculate a phase for subsequent Fourier Transform calculations. Although this mode limits the resolution to approximately 30 cm^{-1}, it enables spectra to be taken rapidly (~ 60 seconds) in order to follow changes in band intensity, which is of utmost importance when studying metastable defects in GaN.

3.2 Scanning electron microscopy

The first scanning electron microscope (SEM) was built by von Ardenne in 1938, while the first commercial SEM appeared in 1965.

The SEM (LEO Stereoscan 440) consists of an electron source, quite often a tungsten filament as shown in figure 3.3. However other filaments may be used for the electron gun. These include lanthanum hexaboride (LaB_6) and a field-emission source. A current of ~ 2.5-3 A is passed through the filament. As a result the filament is heated and the electrons acquire enough thermal energy to overcome their work function and are thermally emitted from their source. In order to maximize the lifetime of the filament it should be heated slowly before operation i.e. the current should be increased gradually in small increments to the operating value and then reduced slowly to zero following completion of the experiments. Also alignment of the filament is vital to ensure optimum results.

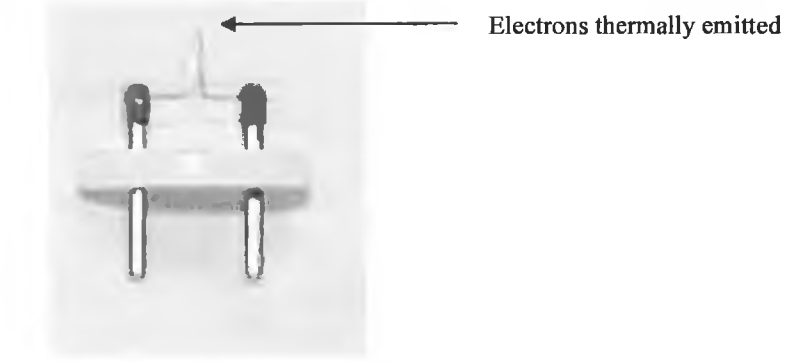

Figure 3.3: Tungsten wire used as electron gun

The electrons emitted from the tungsten (primary electrons) have energy between 5-30 keV, which is considerable less that that used for transmission electron microscopy (TEM). Since electrons have a very short path length in air the entire electron microscope must be under vacuum, generally ~ 10^{-6} torr, while vacuum systems of the order of ~ 10^{-10} torr are required for the field emission source. The standard vacuum for tungsten filaments ~ 10^{-6} is achieved by firstly using a roughing

pump. When the vacuum reaches the required value the turbo molecular pump brings the vacuum down to the required value.

Figure 3.4 shows a simplified layout of the SEM with cathodoluminescence attachment.

The primary electrons are firstly attracted to a positive anode and then focused by a condenser lens system. Adjusting the lens current, and not the lens position as in an optical microscope, controls the focus. The scanning electron microscope also employs an objective lens, which focuses the beam to a fine probe by adjusting the lens current. The final size of the focused electron probe ultimately determines the resolution obtainable.

The image in a scanning electron microscope is obtained by scanning the electron probe over the sample in a television type raster, collecting the required signal and displaying it on a monitor after the required amplification and processing. The image in a SEM is collected sequentially for each data point in turn as the electron probe is scanned across the surface of the sample under investigation. This is in complete contrast to the TEM where the image is focused by an objective lens and a set of other imaging lenses enlarge the final image [Brandon & Kaplan 1999].

The scanning speed of the beam may be reduced or increased, depending on the sample. Generally for better quality images a slow scan speed is desired. This is achieved by increasing the pixel dwell time and therefore allowing the beam to delay on each point for longer, thus increasing the signal from that point. For instance a very fast scan would correspond to a scanning frequency of 15 MHz while a slower scan corresponds to a frequency of about 460 Hz.

The scanning electron microscope may also operate in spot mode. That is the beam is placed on a spot and the signal is collected from that spot. This can be particularly useful for x-ray analysis as compositional information may be obtained from a spot, determined by the probe size. It also has applications in cathodoluminescence where the optical quality of a spot may be examined or depth profiling analysis may be performed as illustrated in figure 4.4. The sample is mounted on a stage, which allows good mechanical movement in the x, y, z-axes as well as a facility for tilt and

rotation. The samples may be analysed from 5 K to 300 K using a suitably designed sample stage, as described in section 3.2.3.

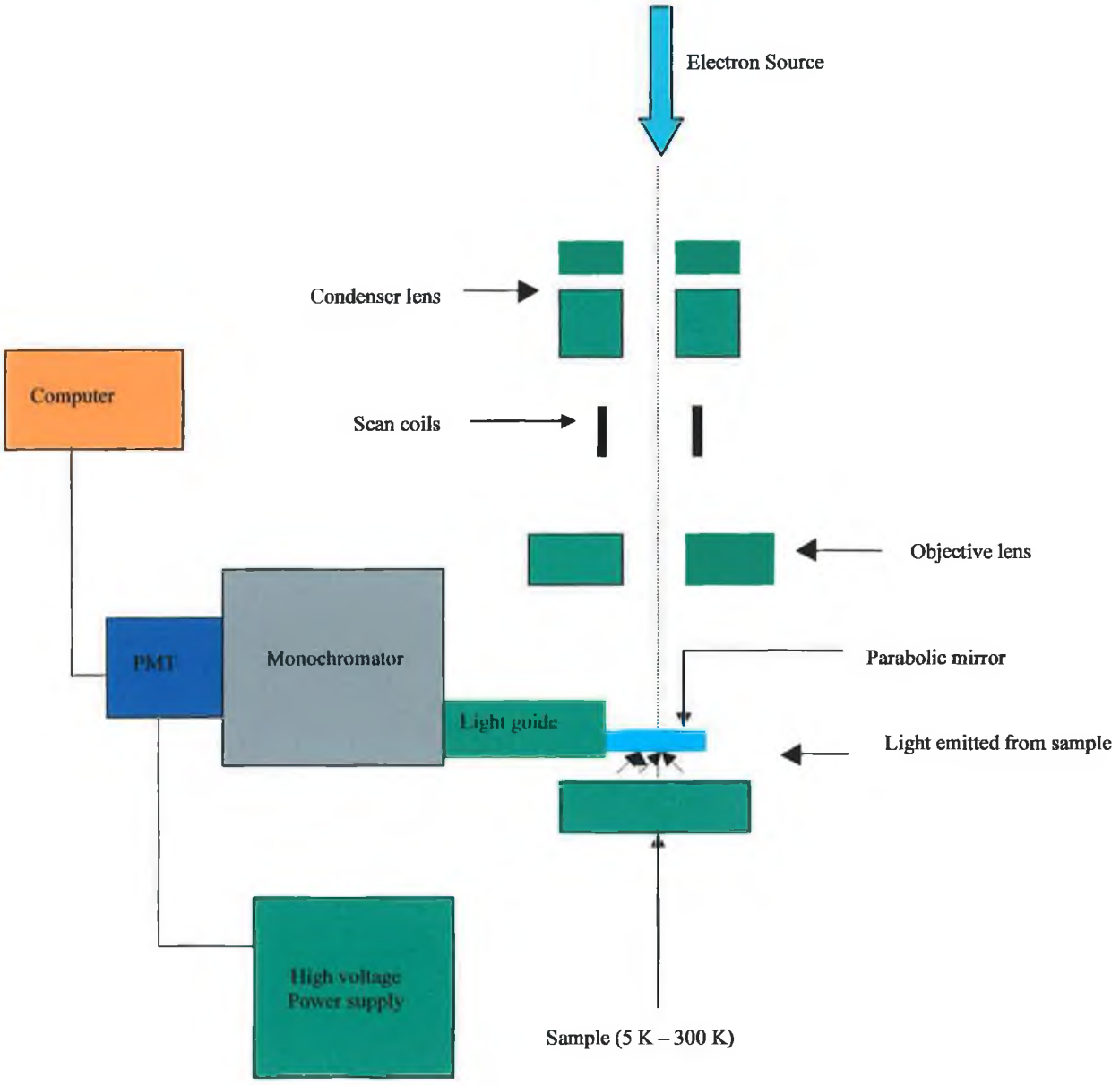

Figure 3.4: Components of a scanning electron microscope with cathodoluminescence attachment

3.2.1 Spatial resolution of the SEM

The understanding of wavelike properties of electrons is vital for an appreciation of many applications. The scanning electron microscope is no exception. The more familiar technique of optical microscopy has many disadvantages as the ultimate resolution obtainable is limited by the wavelength of the light used. As a result optical microscopes cannot resolve details much less than typically 1 μm in size.

For electrons on the other hand the wavelength of the electrons waves depends on the momentum of the particles as defined by the de Broglie principle [Eisberg & Resnick 1985]:

$$\lambda = \frac{h}{mv} \tag{3.7}$$

where h is Planck's constant, m is the electron mass, and v is the electron velocity. If the accelerating voltage of the electrons is given by V, then the kinetic energy is given by:

$$\frac{1}{2}mv^2 = eV \tag{3.8}$$

where e is the electron charge.

Therefore the electron wavelength is given by:

$$\lambda = \frac{h}{\sqrt{2meV}} \tag{3.9}$$

In particular we can see that as the accelerating voltage is increased, the wavelength is reduced in proportion. It is therefore possible to vary the resolution of the scanning electron microscope to view structures far smaller than that obtainable by optical microscopy by increasing the acceleration voltage.

Typically electron microscopes operate at wavelengths a thousand times smaller than that of optical microscopes. Such wavelengths are smaller than the size of atoms and with some careful considerations some atoms may be made visible, although in

practice this process is quite challenging as the process is severely hampered by several lens aberrations. The factors that limit the resolution achievable in practice are now discussed.

3.2.2 Resolution limits and lens aberrations

Although resolution of the order of 100's of nm's is routinely obtainable, further resolution to the atomic level is quite difficult due to a number of limits and aberrations which will now be the subject of a short discussion [Brandon & Kaplan 1999].

Diffraction limit on resolution

The diffraction limit on resolution is defined by the Raleigh criterion:

$$\delta = \frac{0.61\lambda}{\mu Sin\alpha} \qquad (3.10)$$

Where δ is the diffraction limit on resolution, λ is the wavelength of the radiation, μ is the refractive index of the medium, and α is the aperture half angle.

Spherical aberration

If a parallel beam of electrons are incident on an electromagnetic lens, but at a distance from the optic axis, they will be brought to a focus at a point on the optic axis which depends on their distance from it. For instance a beam further away from the axis will be brought to focus at a point closer to the lens. Similarly a beam closer to the axis will be brought to focus at a point further away from the lens. Therefore the plane of best focus will be a disc of least confusion, as shown in figure 3.5, and its size will depend on the width of the incident beam.

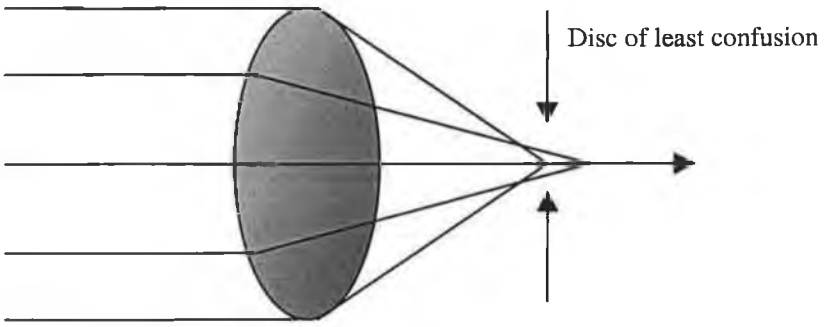

Figure 3.5: Formation of a disc of least confusion

The radius of the disc of least confusion constitutes an aberration-dependent limit on the resolution, which is approximately:

$$\delta_s \approx C_s \alpha^3 \qquad (3.11)$$

Where C_s is the spherical aberration coefficient of the lens and α is the angular aperture of the object.

Chromatic aberration

Chromatic aberration arises due to the fact that electrons with higher energy are less deflected by a magnetic field than those of lower energy. Therefore the higher energy electrons are brought to focus at a point further from the lens than those of lower energy. Once again this leads to a disc of least confusion similar to that of figure 3.5, but this time dependant on the energy spread of the incident beam.

If electrons are thermally emitted, then the relative energy spread may be defined by:

$$\frac{\Delta E}{E_0} = \frac{kT}{eV} \qquad (3.12)$$

Where k is the Boltzmann constant, T is the temperature, e is the electronic charge and V is the acceleration voltage.

Lens astigmatism

The performance of a scanning electron microscope is very much dependant on the alignment of the various components within the microscope column. The objective lens is very sensitive to misalignment, while the axial asymmetry of this lens is very sensitive to minor changes within the microscope, such as size and position of the sample or small amounts of contamination. This may cause a variation in the focal length about the optic axis, resulting in two principal focal positions giving two line foci at right angles.

As seen the resolution of the SEM is limited by the above factors, therefore resolution to the atomic level is not possible. However the SEM offers far better resolution than that obtainable by optical microscopes and is therefore an important tool in the analysis of semiconductors. An important signal of interest is the cathodoluminescence signal and the apparatus used together with the SEM is now described.

3.2.3 Cathodoluminescence apparatus

When a beam of keV electrons are incident on a semiconductor a number of useful signals may be obtained. Figure 3.6 summarizes this process. The focus of this work will be on the cathodoluminescence signal.

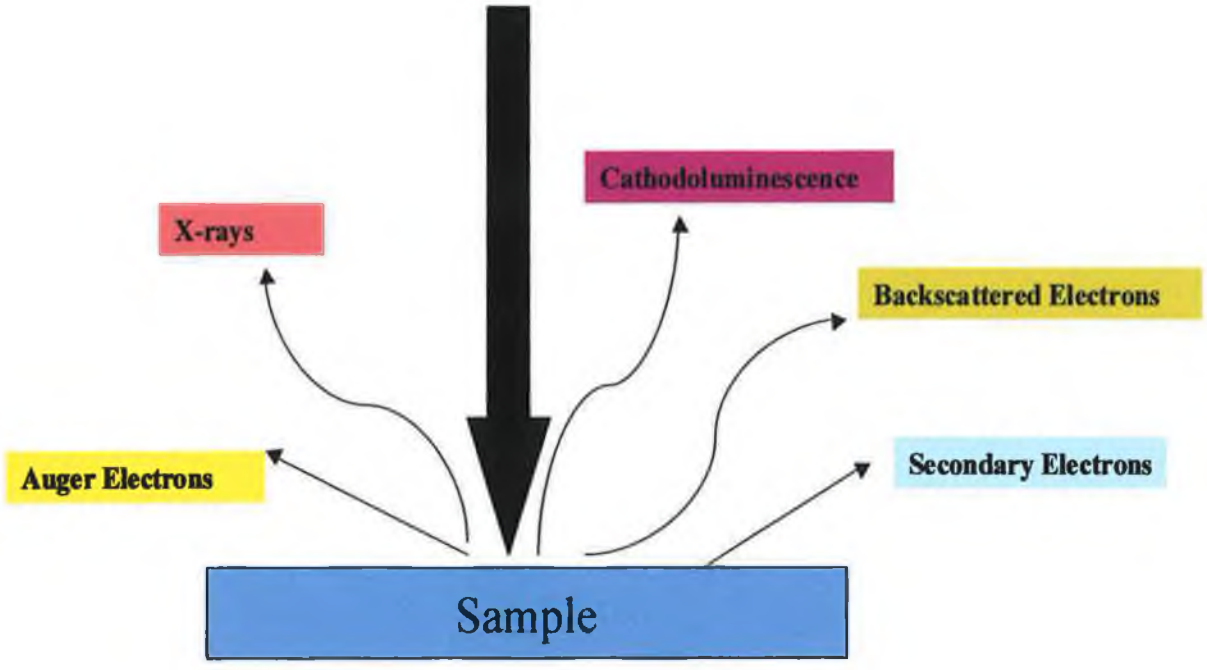

Figure 3.6: Signals produced when an electron beam is incident on a sample

Cathodoluminescence is defined as the emission of electromagnetic radiation as a result of electron bombardment. From this signal one may obtain information on the spatial dependence of luminescence at a sub-μm level and obtain a correlation between structural and optical properties. The cathodoluminescence apparatus is commissioned on the SEM as shown in figure 3.4. Figure 3.7 shows the CL-SEM laboratory with the various components which are discussed below.

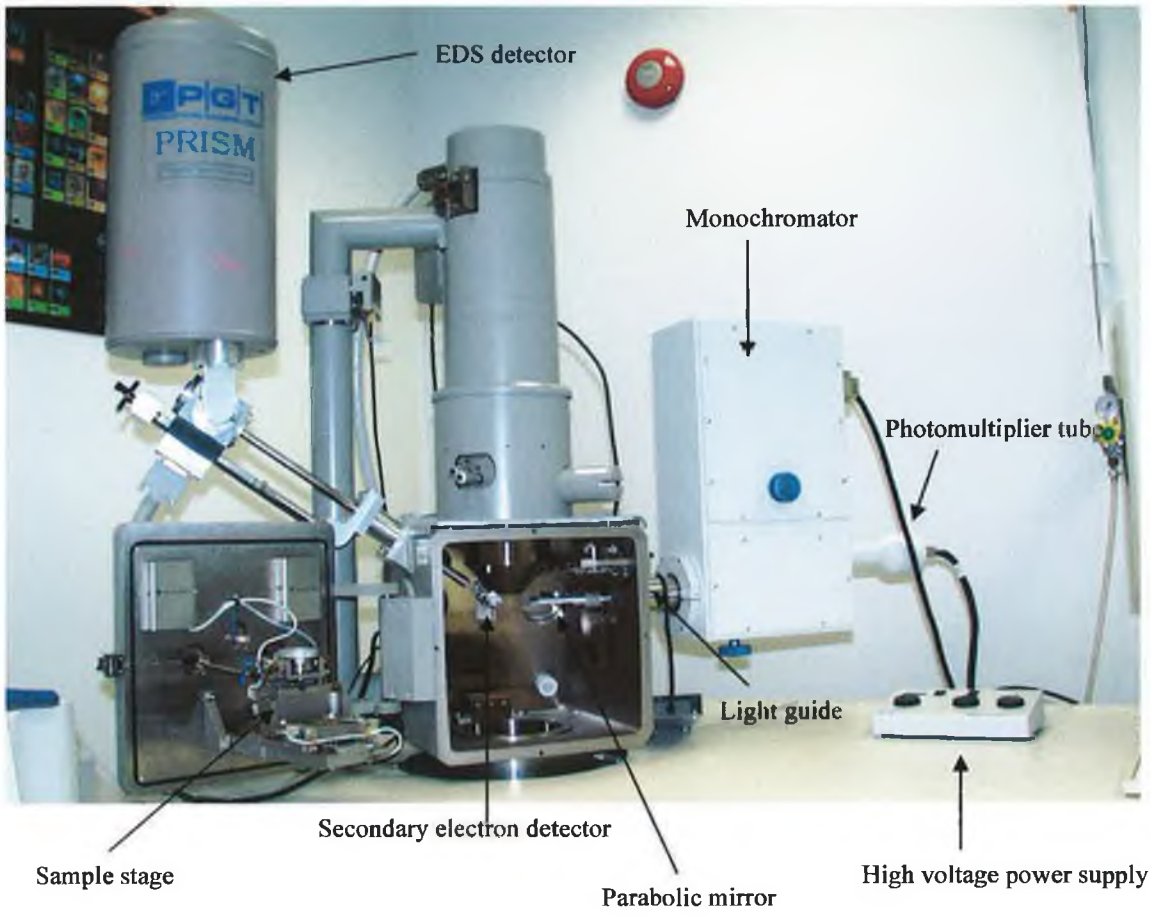

Figure 3.7: Cathodoluminescence spectroscopy laboratory

Parabolic mirror

A parabolic mirror with a 1 mm diameter hole in the top, see figure 3.8, allowing the electron beam to pass through is a vital component in the CL-SEM apparatus. The incident electrons excite luminescence and while some of the photons will escape back up the hole the collection efficiency of the mirror is quite high ~ 75% [Gatan UK operator handbook 2001]. A light guide is present to keep the mirror in place under the pole pieces and the retractable system allows the light guide to be moved back from under the pole pieces when not in use to avoid collision with detectors, large samples and the stage. The focal length of the mirror is 1 mm. Great care must be taken in order to ensure that the sample to mirror distance is exactly 1 mm. The photons collected are transferred via highly reflecting mirrors to the monochromator where the luminescence may be examined.

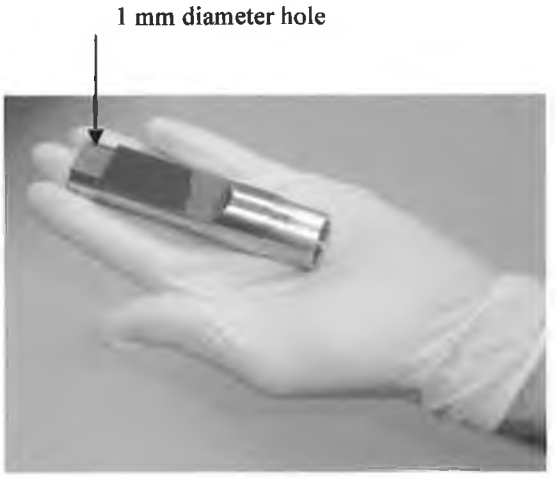

Figure 3.8: Parabolic mirror for collecting luminescence

Monochromator

The monochromator is a Czerny-Turner configuration of focal length 300 mm as outlined in figure 3.9. The light collected is focused onto an input slit. It is then collimated by a concave mirror, which then reflects it onto a diffraction grating with 1200 lines per mm and blazed for operation at 500 nm. The grating diffracts the beam and by rotating about its axis, a range of wavelengths can be diffracted and focused by the second mirror onto the output slit.

The ability of the grating to separate adjacent spectral lines of average wavelength λ is known as the resolving power. It may be expressed as a dimensionless quantity [Palmer 2000]:

$$R = \frac{\lambda}{\Delta\lambda} \qquad (3.13)$$

where $\Delta\lambda$ is the limit of resolution.

The spectrometer may act in two modes of operation. Panchromatic, where all of the light collected from the sample bypasses the spectrometer to the photomultiplier tube and an image (in the detector range) is displayed. Alternatively, if a dominating wavelength is present, such as the bandgap in a direct bandgap material, the grating may be set to this wavelength and the associated luminescence directed to the exit

slits. This may be imaged and is known as monochromatic imagining. The knobs for adjusting the mirrors for panchromatic or monochromatic mode, as well as the adjustments for the slits are located at the rear of the monochromator in figure 3.7.

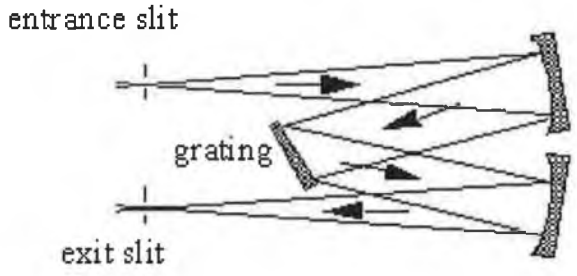

Figure 3.9: Czerny – Turner configuration monochromator [Palmer 2000]

Photomultiplier tube detector

The detector used was a room temperature photomultiplier tube with a preamplifier and magnetic shield. The tube screws into a light tight housing, which is attached to the monochromator, as shown in figure 3.7. It has a spectral range in the region 185 to 850 nm and is most sensitive to the blue part of the spectrum. A high voltage power supply, capable of supplying ~ - 1000 V is used to control the collection of the photomultiplier tube. There also exists on the high voltage power supply a facility for adjusting brightness and contrast of images.

A photomultiplier tube works on the principle that an incident photon is absorbed by the photocathode that in turns emits photoelectrons as in the photoelectric effect. Electrons are directed by an electric field towards a dynode. For each incident electron a number of secondary electrons are emitted. This process is repeated a number of times, depending on the number of dynode plates. At the end of the tube the anode collects the electrons and provides the measured signal current.

DigiScan hardware

The DigiScan unit, not visible in figure 3.7, allows the Gatan software to take control of the beam scanning from the LEO software. This allows added functionality to the CL-SEM facility. For instance line-scanning may be performed. To do this the user

draws a straight line across the sample, using the Region of Interest (ROI) tools in the software, from which the information is required. Then setting the grating to the particular wavelength, the beam then scans a line across the sample and monitors the intensity of the desired wavelength as a function of position. The DigiScan also allows for capturing and processing SEM and CL images.

Low temperature stage

The low temperature stage, shown in figure 3.10, allows the analysis of samples between 4.2 K and room temperature. It allows the accurate movement of the sample under the optical column in the x, y, and z-axes. It operates by controlling the continuous flow of liquid helium from the storage dewar to the cold block located on the low temperature stage as illustrated in figure 3.10.

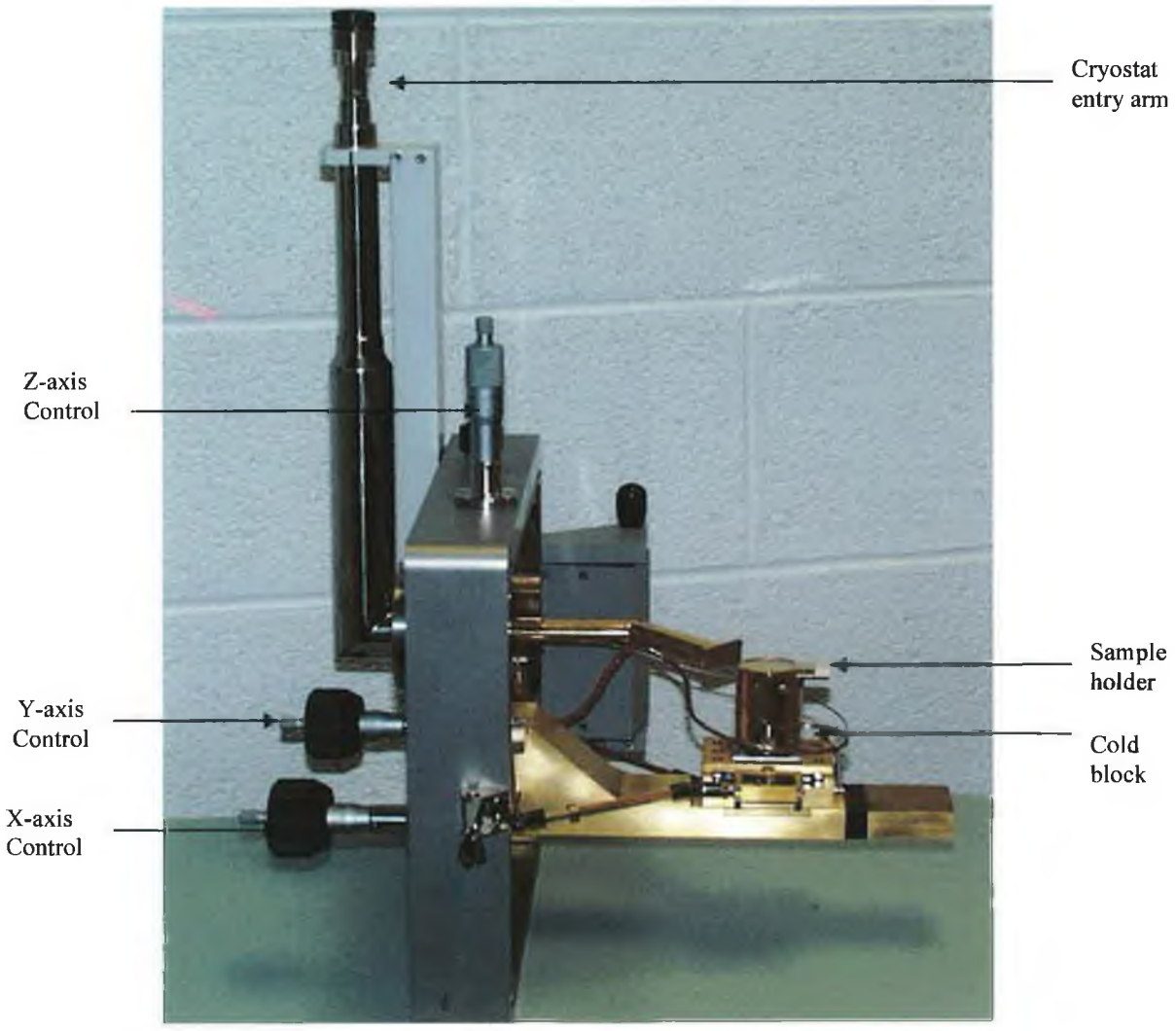

Figure 3.10: Low temperature cathodoluminescence stage

The liquid helium flows through the heat exchanger, attached to the cold block, where the temperature is measured by a rhodium iron sensor [Gatan UK Operator handbook 2001]. Also fitted to the cold block is a heater. The cold block contains a detachable sample holder. After leaving the heat exchanger, the helium (now gas) is used to cool the radiation shield on the cold block and then after passing through the flexible capillaries, cools the shield mounted on the cryogen feedthrough. It then passes along the outside of the coaxial transfer tube. Figure 3.11 shows a schematic of the entire setup.

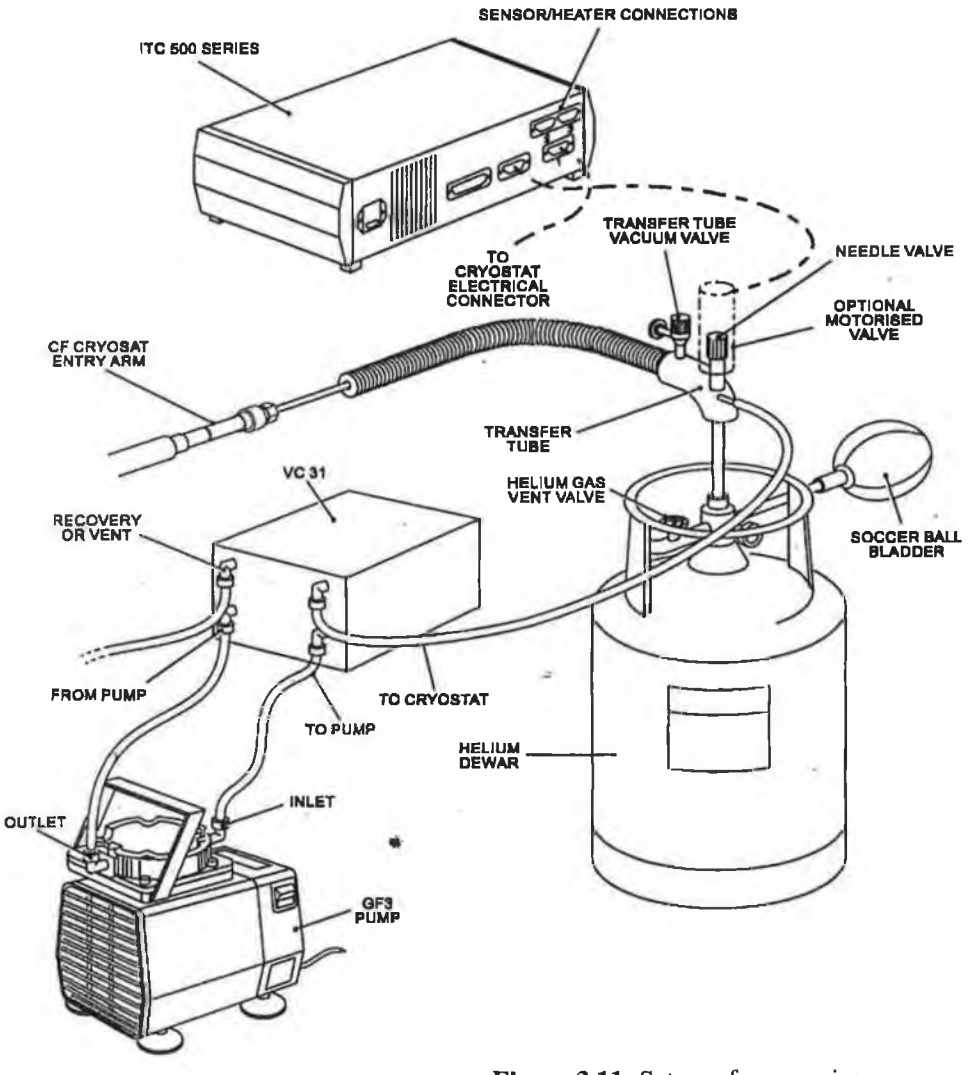

Figure 3.11: Set up of cryogenics
[Gatan UK Operator handbook 2001]

3.2.4 Formation of cathodoluminescence radiation

The three fundamental processes resulting in the emission of cathodoluminescence radiation are the generation, motion, and recombination of excess charge carriers. These factors shall now be the subject of a short description.

3.2.4.1 Generation of excess carriers

Incident electrons impinging on a semiconductor lose energy as their path length increases and eventually stops. The mean rate of energy loss per unit path length S in the solid is described by the Bethe expression [Yacobi & Holt 1990]:

$$\frac{dE}{dS} = -2\pi e^4 N_A \frac{\rho Z}{EA} \ln\left(\frac{1.166E}{j}\right) \tag{3.14}$$

where e is the electron charge, N_A is Avogadro's constant, ρ (g/cm^3) is the density of the material, A (g/mol) is the atomic mass, Z is the atomic number, E (keV) is the mean electron energy , and j is the mean ionization potential.

The incident electron beam undergoes a number of random elastic and inelastic scattering events. As a result it is not possible to estimate the trajectory for an individual electron. However, as a result of these scattering events it is possible to estimate an excitation volume. The range of the incident electrons in the crystal is defined by [Kanaya & Okayama 1972]:

$$R_e(\mu m) = \frac{0.0276A}{\rho Z^{0.889}} E_0^{1.67} \tag{3.15}$$

where E_0 (keV) is the incident beam energy, A (g/mol) is the atomic mass, ρ (g/cm^3) is the density and Z is the atomic number. Figure 3.12 illustrates the range of electrons in GaN as a function of beam energy.

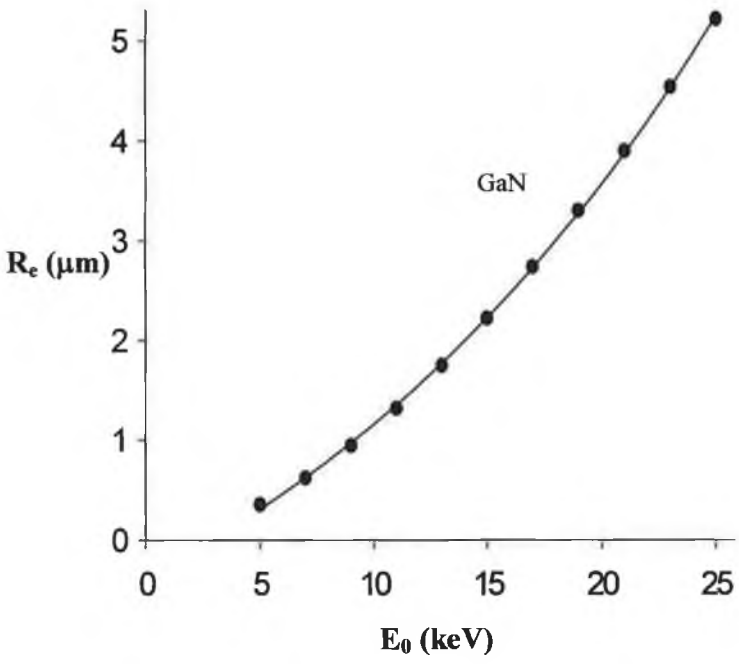

Figure 3.12: Plot of range of electrons in GaN as a function of beam energy using the Kanaya – Okayama model

Monte Carlo simulations were performed using the CASINO program [Drouin *et al.* 1997] for 10, 000 incident electrons using a 25 keV beam. Figure 3.13 illustrates the excitation volumes at these energies for GaN.

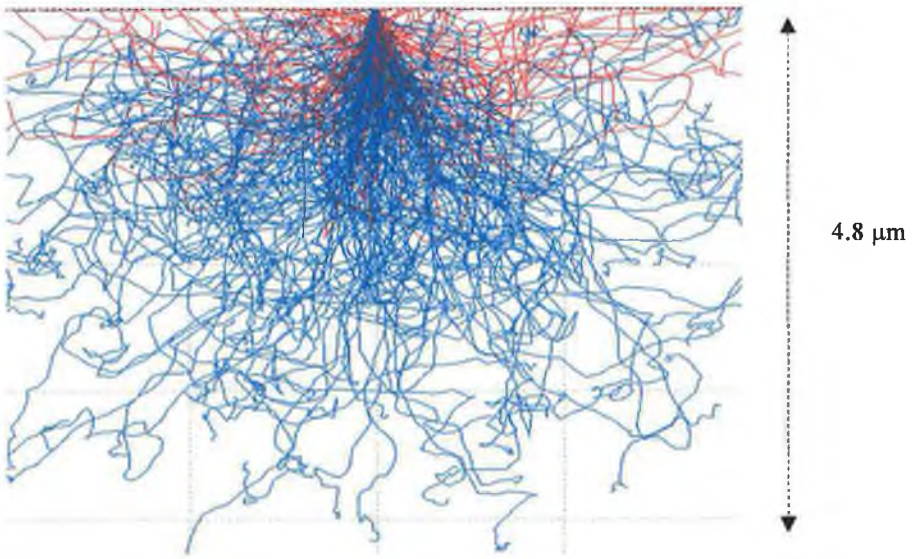

Figure 3.13: Monte Carlo simulations for electron trajectories in GaN at 25 keV. Simulation was performed for 10, 000 electrons with a beam diameter of 50 nm

The blue part of the excitation volume represents the range of primary electrons in the material, while the red lines represent the backscattered electrons.

As can be seen from the Monte Carlo simulations, excess carriers are generated from within an excitation volume in the semiconductor. The number generated is represented by a generation factor [Yacobi & Holt 1990]:

$$G = \frac{E_0(1-\gamma)}{E_i} \tag{3.16}$$

where E_i is the ionization energy and γ is the loss of beam energy due to electron backscattering, while E_0 is the energy of the primary electrons. The ionization energy is that required to create one electron hole pair and is dependent on the bandgap of the material, but independent of the electron beam [Klein 1968]:

$$E_i = 2.8E_g + M \tag{3.17}$$

M is material dependent and is generally $0 < M < 1$.

The general shape of the excitation volume is atomic number dependent as well as depending on the beam energy as shown in figure 3.14.

One of the fundamental differences between cathodoluminescence and photoluminescence spectroscopy is that while one incident photon can generate one electron hole pair, one 20 keV electron can generate a few thousand electron hole pairs.

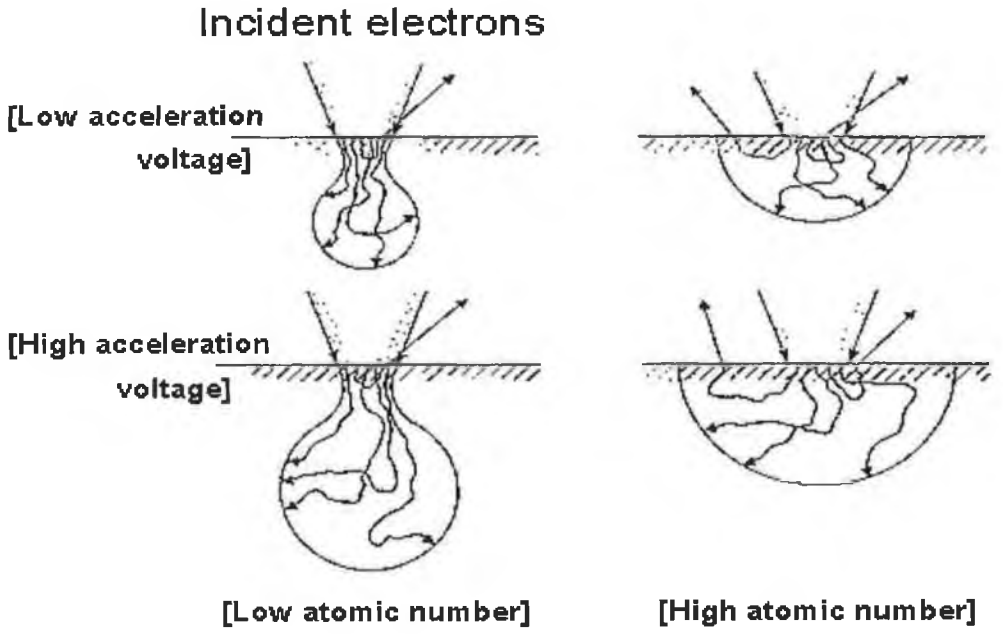

Figure 3.14: Effect of low and high-energy electrons on a semiconductor of low and high atomic number [JEOL]

Generally speaking the following factors ultimately determine the resolution obtainable in CL-SEM:

- probe diameter;
- generation volume;
- minority carrier diffusion length.

3.2.4.2 Motion and recombination of excess carriers

The non-equilibrium charge carriers move by drift and diffusion and then recombine either radiatively or non-radiatively. The CL intensity I_{cl} is proportional to $\Delta n(r)$, the excess minority carrier density per unit volume [Petrov 1996]:

$$I_{cl} = \int_{v} AB\eta(r)\Delta n(r)dV_r \qquad (3.18)$$

Where A and B are correction factors for CL absorption loss inside the object and CL reflection loss at the semiconductor vacuum interface and $\eta(r)$ is the internal quantum efficiency, which is the ratio of the radiative recombination rate to the total

recombination rate, that is radiative plus non-radiative. The internal quantum efficiency is normally expressed in terms of lifetimes as the following [Petrov 1996]:

$$\eta = \left(1 + \frac{\tau_{rr}}{\tau_{nr}}\right)^{-1} \qquad (3.19)$$

where τ_{rr} and τ_{nr} are the radiative and non-radiative carrier lifetimes respectively.

3.2.5 Other SEM signals

Depending on the sample other important SEM signals may also be produced [Brandon & Kaplan 1999]. Many of these are acquired using the detectors shown in figure 3.7. Some of the signals are summarized below.

Secondary electrons

Secondary electrons are those which are emitted from the sample itself as a result of excitation from incident electrons. The electrons emitted are of low energy, typically ~100 eV, therefore their mean free path is very small. As a result they are emitted from the first few nanometers of the material. They are collected with high efficiency, by a low bias voltage, typically ~ 300 V. Secondary electrons are the most useful signal produced. They may be used in the analysis of rough surfaces at high resolution, as objects closer to the detector appear brighter than those further away.

Backscattered electrons

A portion of the incident electrons will interact with the nucleus of the host material and get scattered at angles greater than π. These electrons have energy of the same order of magnitude as the incident ones and originate from within 1 μm of the specimen surface. These signals give very good atomic number contrast, since regions of high atomic number backscatter more primary electrons than regions of low atomic number. Therefore important information on the uniformity of the samples composition may be obtained, as bright areas will generally correspond to elements of larger atomic number.

X-rays

If the incident beam interacts with one of the inner shells of the atom, the resulting photon will be in the x-ray part of the spectrum. An x-ray spectrum may be obtained by scanning the beam over a small area of the sample or else operating in spot mode. The x-ray spectrum yields information about the elements present in the sample, their quantities and distribution.

Auger electrons

This is a non-radiative recombination process, in which the energy released by the recombination of an electron and hole is transferred to a third free carrier (either an electron or a hole). They possess very low energy and are generally emitted from the first few angstroms of the material. Auger electrons are characteristic of elements from which they originate.

3.3 Conclusions

This chapter has dealt with the important considerations behind the characterisation techniques of photoluminescence and cathodoluminescence spectroscopy. Reasons for their extensive use by researchers have been highlighted. These techniques will be used in obtaining experimental data as will be shown in chapters 4 & 5.

4 Cathodoluminescence results

4.1 The luminescence of GaN

The luminescence spectrum of GaN normally consists of three distinct regions. The bandedge luminescence appears as a sharp line near ~ 3.4 eV. Two main broad defect bands have been observed in GaN. The commonly observed yellow band (YB), centred at 2.2 eV has been widely observed in many samples [Toth *et al.* 1999], [Ogino *et al.* 1980].

The yellow band in GaN has been the subject of considerable debate. It is normally a very broad band ranging from about 480 to 640 nm, which is centred at about 550 nm (~ 2.2 eV). The occurrence of this broad band may be explained using the CC model as outlined in section 1.5.

It is generally accepted that the origin of this band is due to one of two possibilities. It has been proposed to be due to a transition between a shallow donor D_{sh} and a deep acceptor A_{de} [Ogino *et al.* 1980] located at:

$$E \approx E_v + 0.86eV \qquad (4.1)$$

Another model proposes a deep donor to a shallow acceptor recombination producing luminescence at [Glaser *et al.* 1995]:

$$E \approx E_c - 1.0eV \qquad (4.2)$$

However the deep donor and shallow acceptor are in this case the subject of debate. Both of these models are illustrated in figure 4.1.

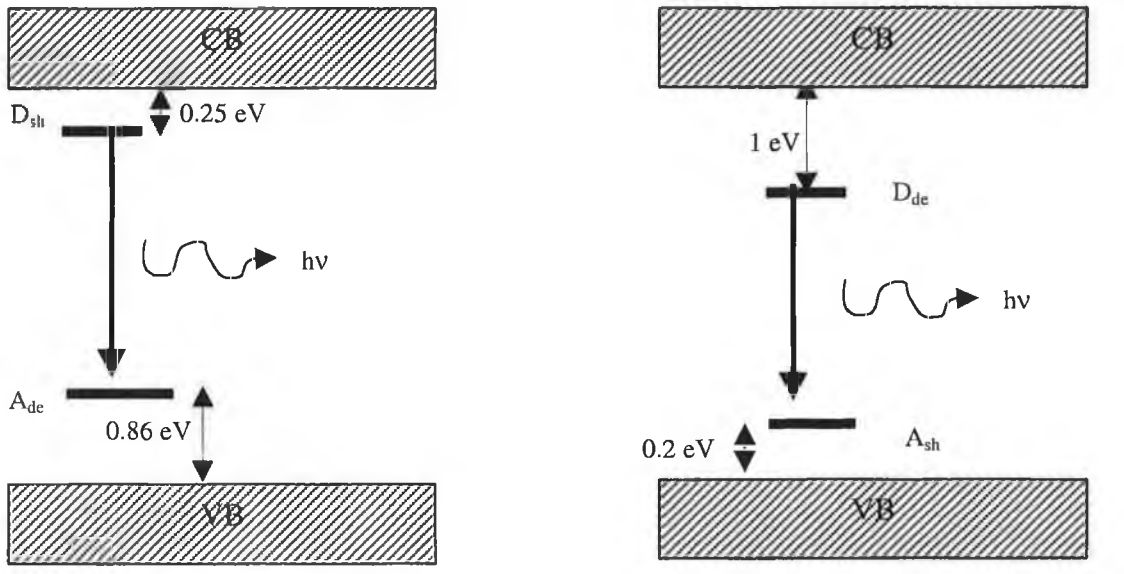

Figure 4.1: Proposed models for origin of yellow band in GaN by (a) Ogino *et al.* and (b) Glaser *et al.*

Generally speaking many researchers still support these theories [Reshchikov *et al.* 2000], [Godlewski *et al.* 2000], [Shalish *et al.* 1999]. The deep acceptor is thought to be a Ga vacancy (V_{Ga}^{3-}) [Xu *et al.* 1998], [Dhar *et al.* 2002]. The precise origin of the shallow donor on the other hand is unclear. However researchers have suggested that it may be due to substitutional oxygen (O_N^+) and silicon (Si_{Ga}^+) [Mattila *et al.* 1997]. Recently another broad band centred at 2.9 eV has been observed in many samples. It is thought to be due to a metastable defect [Xu *et al.* 1998]. Also of interest is the inter relationship between the 2.2 and 2.9 eV bands in GaN [Xu *et al.* 1998], [Kim *et al.* 1999]. A discussion of this will be the subject of chapter 5.

In this chapter cathodoluminescence was used to investigate the optical quality of GaN grown on sapphire. Of particular interest is the epitaxial lateral overgrowth process, which is a far superior technique for the reasons explained in section 2.3.2. We investigate both ELO and non-ELO grown GaN at room and low temperature and support our data with published topography measurements from a collaborating group.

4.2 Room temperature cathodoluminescence of GaN

Room temperature cathodoluminescence was applied to the study of non-ELO and ELO GaN. The following will facilitate a comparison between the optical qualities of both materials.

4.2.1 Application of room temperature CL-SEM to non-ELO GaN

The first sample investigated consists of a thin (50 nm) GaN buffer layer grown on a 440 μm thick c-plane sapphire substrate at 550^0 C using MOVPE. Following this a 1.2 μm epilayer was deposited. The sample was grown by INTEC at the University of Gent, Belgium.

A room temperature cathodoluminescence measurement from this sample is shown in figure 4.2. The measurement was taken using a focused electron beam operating in spot mode with 8 keV electrons, corresponding to information from the first 0.75 μm of the epilayer.

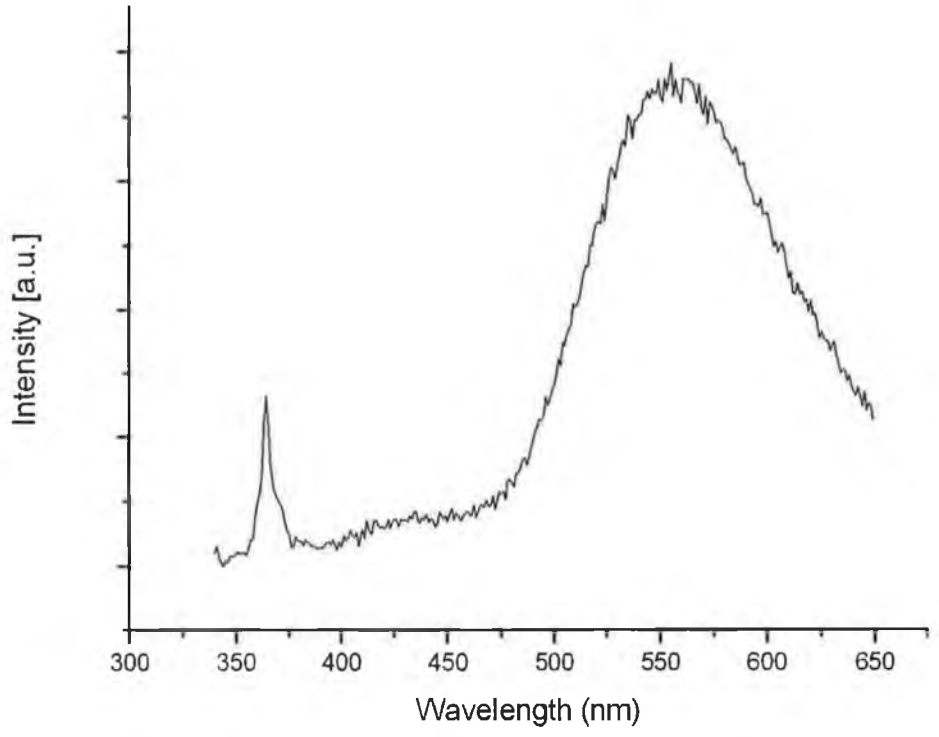

Figure 4.2: Cathodoluminescence spectra from non-ELO GaN using an 8 keV beam

The measurement clearly shows relatively low bandedge intensity when compared to the yellow defect related emission centred at ~ 550 nm.

The defect related yellow luminescence dominates the spectrum, the resulting ratio of ultraviolet to yellow peak intensity being 1:3.2. Previous topography work on this sample [McNally *et al.* 2001] supports the idea that the poor optical quality of this sample is due to its poor structural properties.

Figure 4.3 (a) shows a panchromatic CL-SEM image of the sample. That is all the light from the sample was incident on the detector, without undergoing dispersion through the monochromator. The image shows a variation of both bright and dark regions, corresponding to high and low luminescence efficiency.

Figure 4.2 (b) shows a monochromatic image of the sample taken at the bandedge wavelength ~ 364 nm. That is the grating was set using the Gatan software to 364 nm and the light collected by the parabolic mirror was dispersed through the grating and focussed on the exit slit. This image is of particular interest as it shows the luminescence originating from the grains. In contrast the areas around the grains (grain boundaries) appear dark. This indicated that the desired bandedge luminescence comes from the grains and possibly suggests that the dark areas are due to defects, possibly originating from the high dislocation density as discussed in section 2.3.1. The yellow band (~ 550 nm) was also imaged, as in figure 4.2 (c). This does not show the luminescence originating from the grains as in figure 4.2 (b). It is not clear from the image from which regions this luminescence is originating.

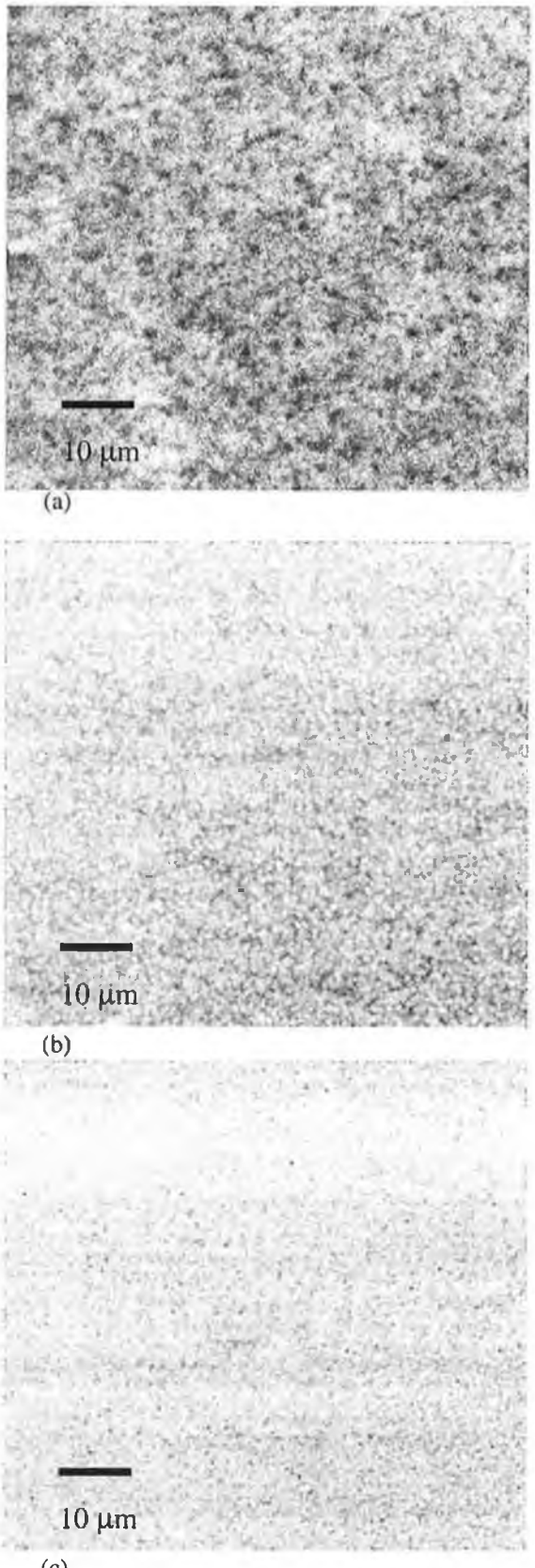

Figure 4.3: (a) panchromatic (b) 364 nm monochromatic and (c) 550 nm monochromatic cathodoluminescence images of the non-ELO material.

One of the main advantages of cathodoluminescence over other characterisation techniques is that it allows depth profiling to be performed. This means that the energy of the incident electrons may be changed and therefore important information about the crystals optical quality may be obtained as a function of depth into the crystal. Accurate simulations/calculations may be performed [Drouin *et al.* 1997], [Kanaya & Okayama 1972], [Hoff *et al.* 1971] allowing the user to estimate the electron penetration depths and excitation volume caused by the incident electron beam in a variety of situations.

Figure 4.4 (b) depicts cathodoluminescence spectra recorded at three different depths within the sample. All spectra were normalized to the same bandedge intensity in order to illustrate the behavior of the yellow luminescence with depth. As the electron beam, operating in spot mode, probes closer to the interface between GaN and sapphire the defect related yellow emission increases with respect to the ultraviolet bandedge emission. The incident electrons of energies of 5, 8 and 12 keV were calculated by the Kanaya Okayama model [Kanaya & Okayama 1972] to correspond to a range of 0.34, 0.75 and 1.2 μm respectively are illustrated in figure 4.4 (a).

The ratio of the ultraviolet to yellow luminescence increases from 1:0.357 at a depth of 0.34 μm to 1:5 at 1.2 μm corresponding to information close to the GaN Al_2O_3 interface as illustrated in figure 4.4 (b). It is possible that the lattice mismatch between the substrate and epilayer, as discussed in section 2.3.1, plays a significant role in the origin of the yellow luminescence. The yellow band has previously been reported to be due to extended crystalline defects inside the grains and at low angle grain boundaries [Ponce *et al.* 1996].

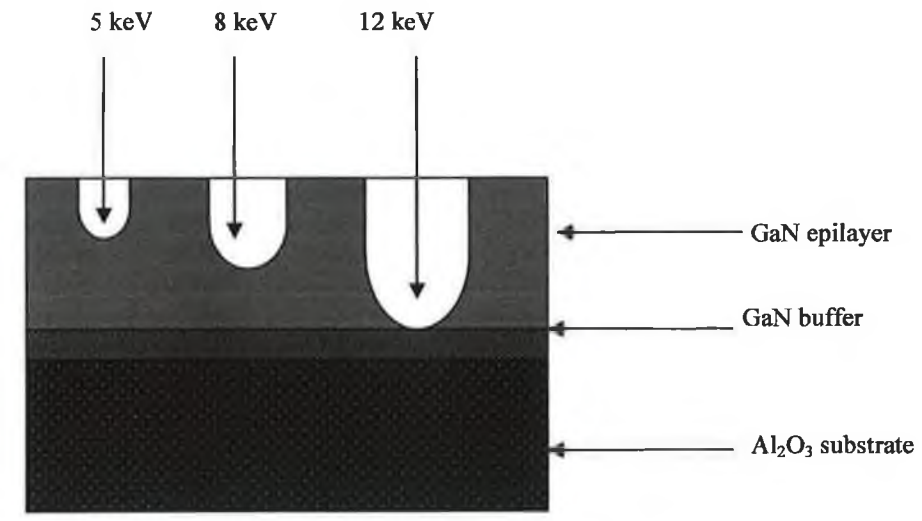

(a)

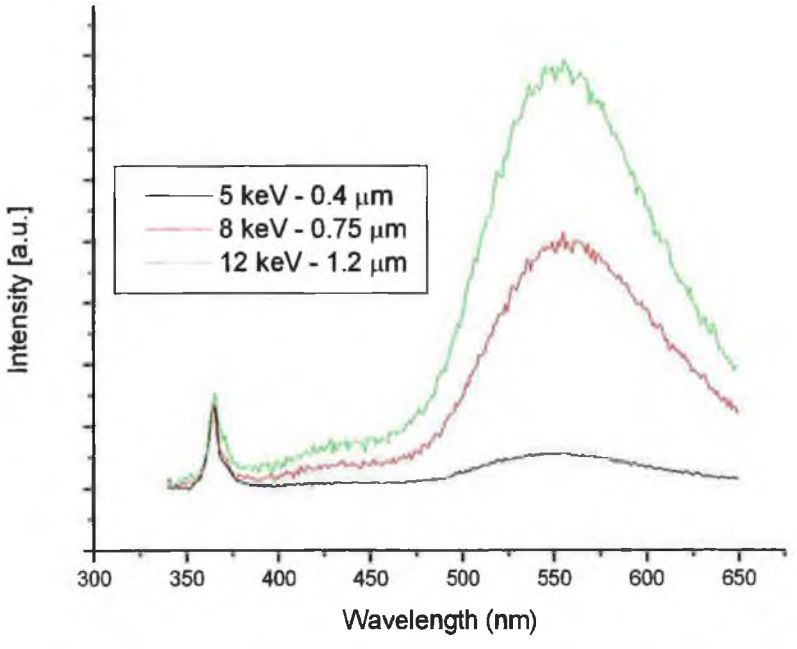

(b)

Figure 4.4: (a) Illustration of sample with incident electrons of different energies and the corresponding excitation volumes in each case and (b) the resulting spectra at each depth.

4.2.2 Application of room temperature CL-SEM to ELO GaN

A current solution to the problem of hetroepitaxial growth of GaN on Al_2O_3 is Epitaxial Lateral Overgrowth (ELO). This technique involves creating openings in a SiO_2 mask to facilitate growth from the underlying seed material. The material grows vertically through the windows and laterally over the mask as shown in figure 2.6. The dislocation density in the resulting epilayer can be 3 or more orders of magnitude lower than in regular hetroepitaxy [Yu *et al.* 1998], [Amokrane *et al.* 2000].

The ELO sample investigated consisted of window openings of 5 μm etched in 100 nm thick SiO_2 stripes deposited using plasma enhanced chemical vapour deposition (PECVD). The GaN was then grown using MOCVD by ELO to a final layer thickness of ~ 6.8 μm. The sample was grown by INTEC at the University of Gent, Belgium.

Figure 4.5 shows a panchromatic image of an ELO sample. The white region indicates luminescence from the region directly over the SiO_2 i.e. this is the region where the GaN has grown laterally over the mask. Adjacent to this bright region is a highly defective dark region recorded from above the window openings in the SiO_2.

The electron beam was focused onto a bright ELO stripe, such as that in figure 4.5 and a spectrum was acquired from the spot. The resulting spectrum is shown in figure 4.6.

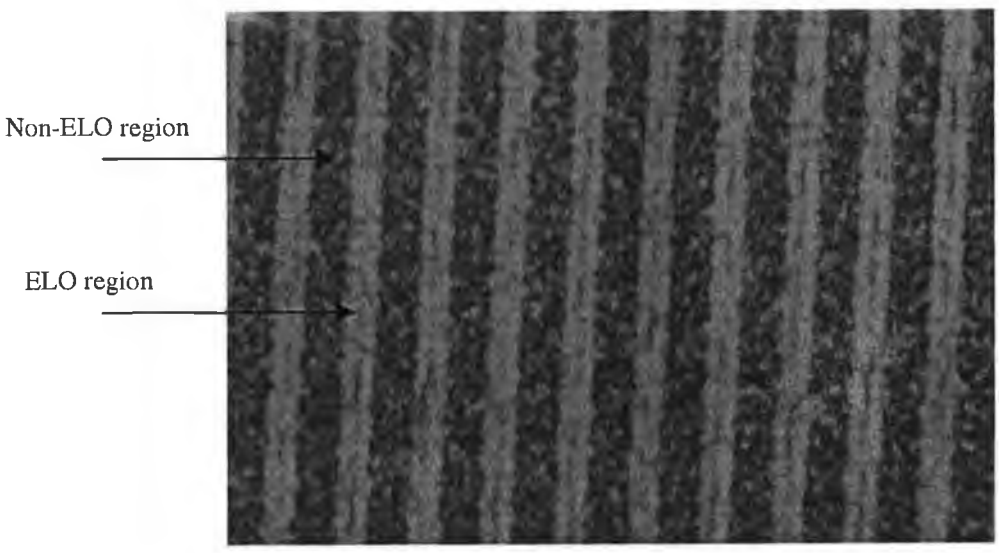

Figure 4.5: Panchromatic cathodoluminescence image of ELO GaN

As can be seen from the figure, the resulting spectrum consists of an intense bandedge peak and relatively weak defect bands when compared to figure 4.2. The ELO sample has previously been the subject of some topography measurements [McNally *et al.* 2001]. These results showed far superior structural properties when compared to the non-ELO material and hence the superior optical quality.

Thin lines of dark spots are visible in the middle of the laterally overgrown region of figure 4.5. This has also been observed by other research groups [Johnson *et al.* 1999] and thought to be due to the difference in lattice orientation, of the individual laterally overgrown GaN stripes at the point of coalescence, being accommodated as a line of defects or small sub-surface voids; this has been sketched in figure 2.6.

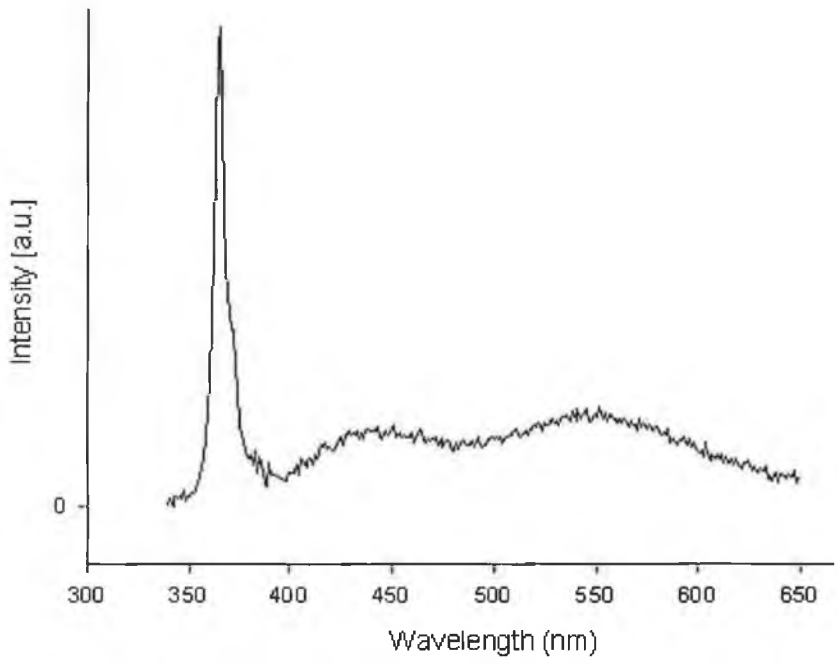

Figure 4.6: Spectra from an ELO stripe from figure 4.5

The panchromatic image in figure 4.5 shows both bright (ELO) and dark (non-ELO regions). A comparison of the optical quality of these regions was performed. The spectra from each region are shown in figure 4.7. As can be clearly seen the spectra from the ELO region is characterised by high intensity bandedge emission and relatively low intensity defect bands, which is consistent with previous measurements [Johnson *et al.* 1999], whereas the non-ELO region has weak bandedge intensity and

relatively intense defect bands. Each spectrum in figure 4.7 has been normalised to the same bandedge intensity to facilitate a comparison between the defect bands.

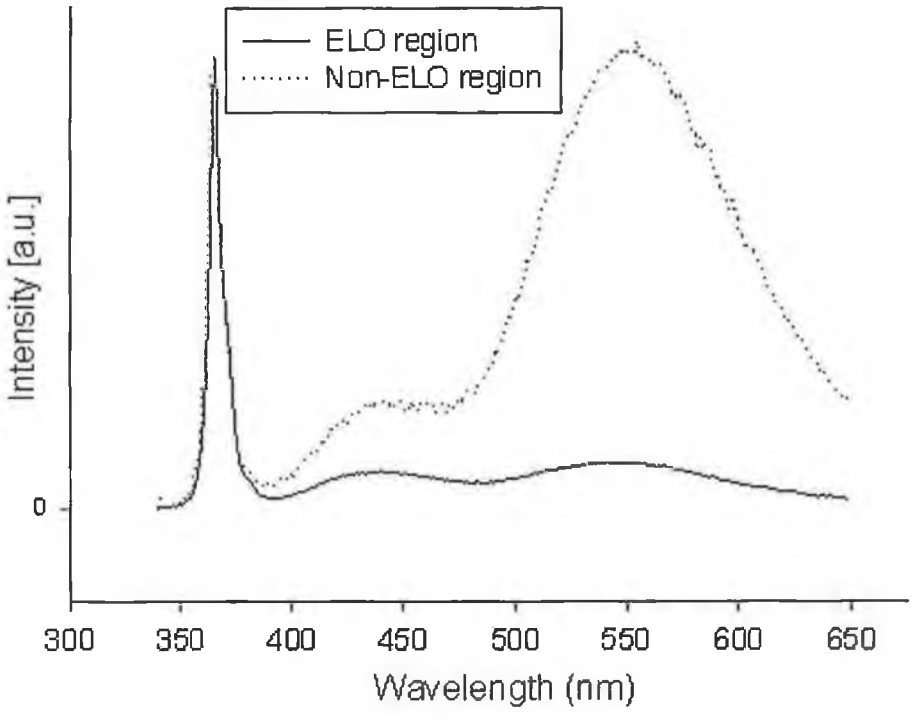

Figure 4.7: Cathodoluminescence spectra taken from ELO and non-ELO regions of figure 4.5

The appearance of a blue luminescence band centred at around 420 nm was noted in our samples. This band has been central to recent research in GaN and will be the subject of discussion in chapter 5.

As discussed previously the ELO technique can lead to a significant reduction in dislocation density in the laterally overgrown layer through mask blocking of vertically propagating dislocations and by means of a redirection of others at the growth front. This effect is clearly seen in figure 4.8 [McNally *et al.* 2001] using TEM images from one of our ELO samples.

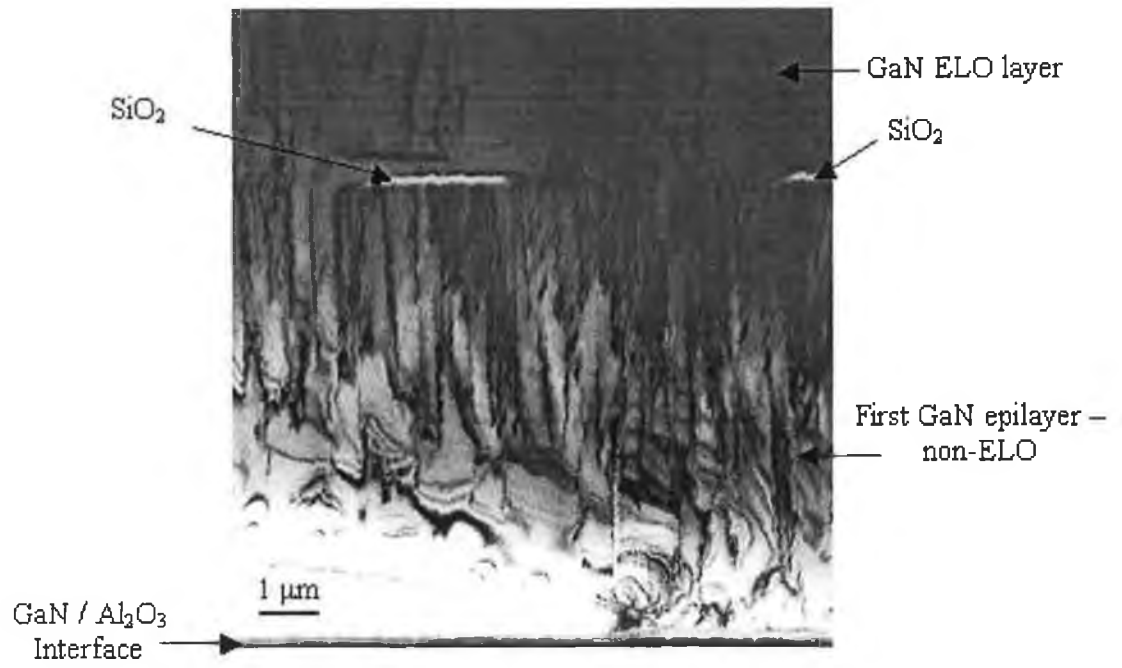

Figure 4.8: TEM image of ELO GaN, illustrating the blocking of vertically propagating dislocations and a redirection of others [McNally *et al.* 2001]

Depth profiling was also performed on the ELO sample. Firstly a panchromatic image of the sample, similar to that in figure 4.5, was obtained for positioning of the excitation source. Once the excitation source was positioned on an ELO stripe, the mirrors were changed to monochromatic mode and the energy of the beam was altered. Incident energies of 8, 15 and 24 keV corresponding to a range of 0.75, 2.14 and 4.7 μm respectively, were used. The resulting spectra are shown in figure 4.9 with the bandedge intensities all normalised to the same value, once again in order to draw a comparison between the defect bands.

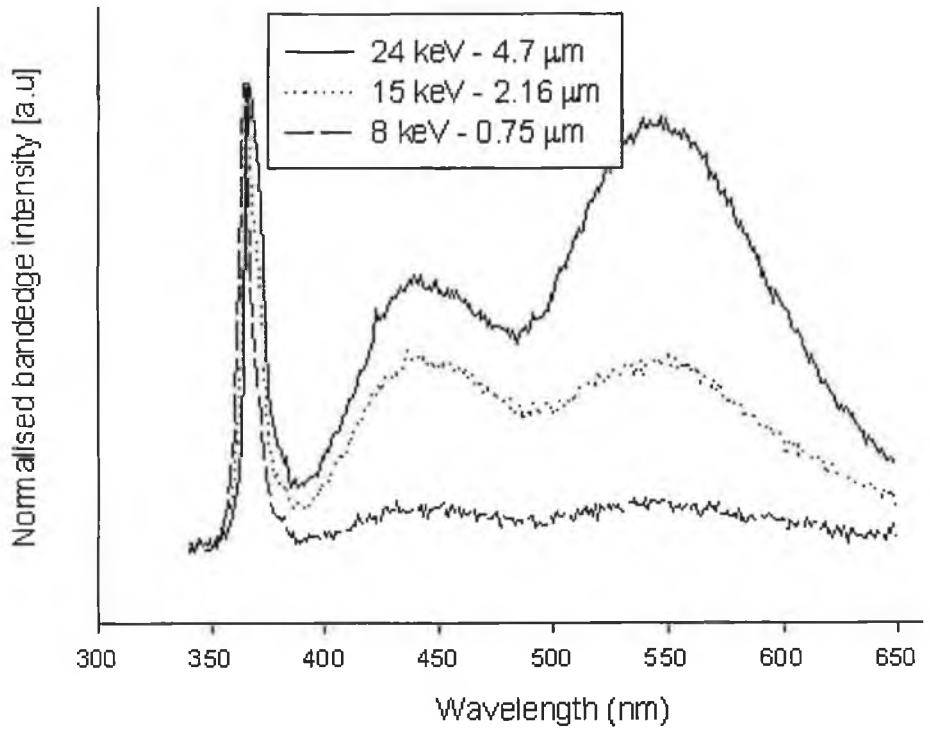

Figure 4.9: Depth profiling on performed on an ELO stripe from figure 4.5

Once again an increasing yellow band was observed with depth. This indicates that the ELO quality improved with distance from the GaN/SiO_2 interface. Most notable in this case is the appearance of a blue luminescence band referred to above. The intensity of this band also increased with depth. The origin of this band has received considerably less attention than the yellow band. It is thought to be due though to a metastable defect, which is discussed in chapter 5.

4.2.2.1 Cathodoluminescence line-scanning

Further evidence for the superior optical quality of ELO GaN may be seen by line scanning across the sample. This was performed as follows. Firstly a panchromatic image of the sample was obtained, the mirrors were then set to monochromatic mode and a spectrum was run, with the slits set to 500 µm. From the spectra the bandedge luminescence was noted to be ~ 364 nm. The grating was then set to this wavelength using the Gatan software and the slits were opened back to 800 µm this resulted in the image shown in figure 4.10.

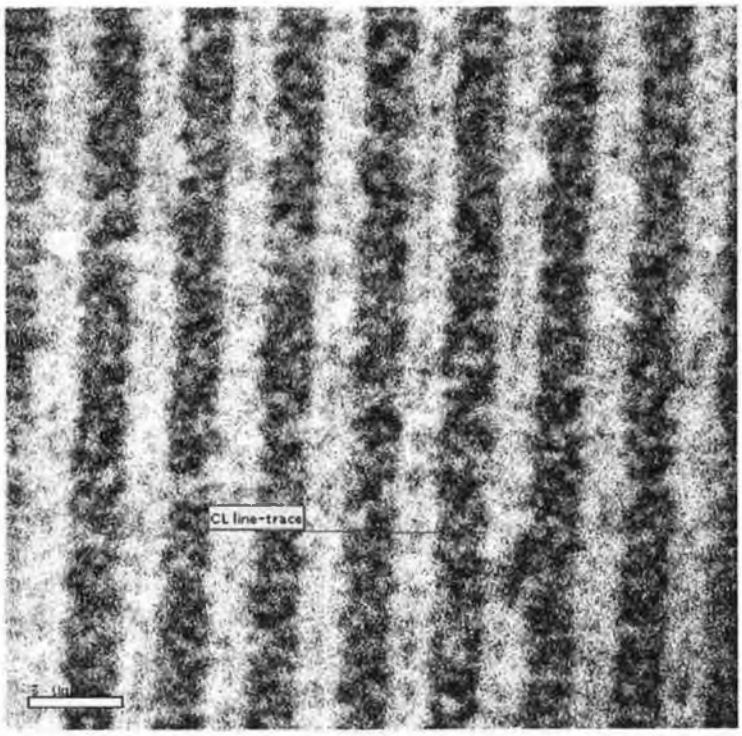

Figure 4.10: Monochromatic cathodoluminescence image of ELO GaN at 364 nm using an electron beam of energy 15 keV, a probe current of 5 nA and 800 μm slits

A horizontal line was then drawn across the image using the ROI tools. A line scan was then performed, with the electron beam scanning a line across the sample. The 364 nm wavelength was therefore monitored as a function of position. The resulting spectrum is shown in figure 4.11.

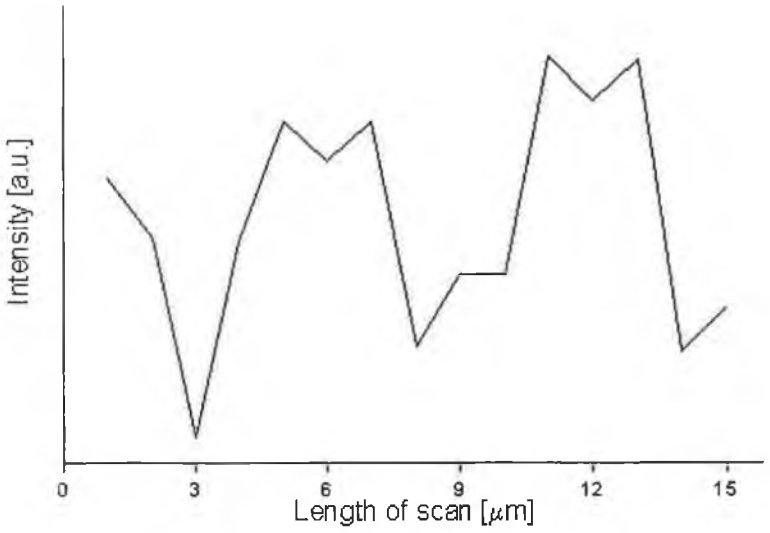

Figure 4.11: Line scan corresponding to region from figure 4.10

It can be seen from the figure that the intensity varies from ELO to non-ELO regions, with higher bandedge luminescence intensity in the ELO regions (bright regions from figure 4.10). As the beam moves to a non-ELO region the intensity is seen to decrease. This is a very useful facility which complements the CL-SEM facility for measuring the variations in luminescence intensity as the beam moves across the material. Once again the spot size of the electron probe becomes an important consideration when deciding how short the linescan can be, as a large defocused beam can only be scanned across a large area.

4.3 Low temperature cathodoluminescence of GaN

Low temperature cathodoluminescence can offer many advantages over room temperature measurements such as:

- Emission bands generally become more intense;
- Thermal broadening is reduced;
- An improved signal to noise ratio;
- More clearly defined energy levels are obtainable.

The bandedge peak can be resolved into well-defined emissions, such as free exciton, and donor and acceptor bound exciton recombination events. Unfortunately, the present resolution (1-2 nm) of the cathodoluminescence system does not allow us to resolve these.

The bandgap is strongly temperature dependent and it shifts to higher energies (longer wavelengths) when the temperature is reduced. This behavior has been described by the Varshni equation [Varshni 1967]:

$$E_g(T) = E_g(0) - bT^2/(T+\theta) \qquad (4.3)$$

where $E_g(0)$, is the energy gap at 0 K, b is an empirical constant, and θ is the Debye temperature at 0 K.

4.3.1 Application of low temperature CL-SEM to non-ELO material

Low temperature cathodoluminescence was applied to the non-ELO sample. The sample was cooled to 20 K and the beam was switched on. The energy of the beam was 5 keV and the probe current was 500 pA. It was noted that a much lower probe current would suffice for low temperature measurements, since at low temperatures the emission intensity was sufficient at this value. The beam was set scanning over the sample and a spectrum was acquired. The resulting spectrum is shown in figure 4.12.

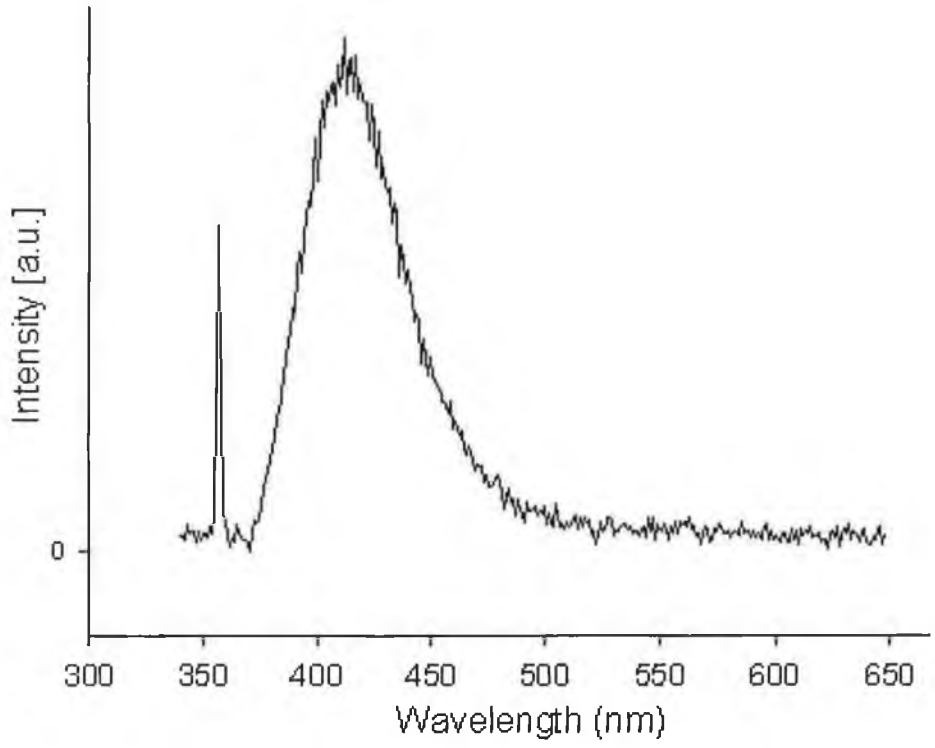

Figure 4.12: Cathodoluminescence spectra recorded at 20 K from non-ELO material

As can be seen the bandedge peak is much narrower due to reduced thermal broadening. Interestingly the yellow band is absent at this temperature and instead a strong defect related blue band was dominant. A number of spectra were acquired from different regions of the sample at 20 K and none showed signs of the yellow band, just the bandedge peak and an intense blue band (all were very similar to that of figure 4.12).

The origin of this blue band is very unclear. Spectra from GaN grown on 6H-SiC [0001] have showed a similar blue band at 80 K [Gruzintsev *et al.* 2001]. This blue band observed in our sample is however not the same as that observed by Gruzintsev whose band ranged from ~ 420-540 nm. This Russian research group has attributed this band to be due to the fact that regions containing a few types of donors and acceptors each with different spectral positions overlap into a broad band such as that in figure 4.12. Also many researchers, including this group have attributed the blue band to a metastable defect and showed a relationship between the blue and yellow bands [Xu *et al.* 1998], [Kim *et al.* 1999], [Brown *et al.* 1999], [Henry *et al.* 2003].

4.3.2 Application of low temperature CL-SEM to ELO material

Low temperature cathodoluminescence was applied to both the ELO and non-ELO regions of the ELO material. These measurements were performed using a 5 keV electron beam and a probe current of 500 pA at 20 K. The electron beam was operated in spot mode and placed on an ELO stripe and spectrum was acquired from that spot. The beam was then placed on a non-ELO stripe and a second spectrum was obtained. Both spectra were normalised to the same bandedge intensity in order to facilitate a comparison between the blue and yellow defect bands from each material. The resulting spectra are shown in figure 4.13.

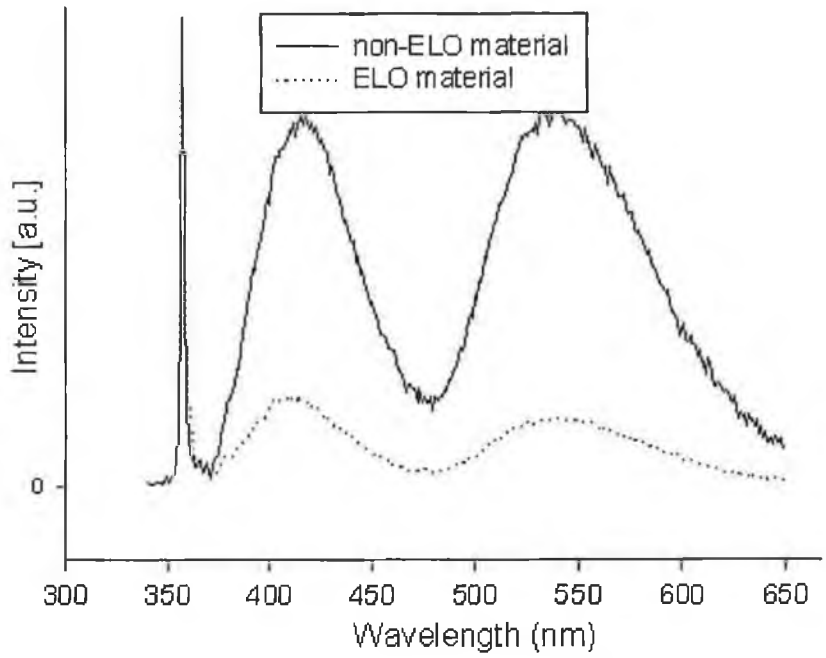

Figure 4.13: Cathodoluminescence spectra taken from ELO and non-ELO stripes of ELO material

As can be seen from the resulting data the non-ELO region possesses much more intense defect bands than the ELO region. In chapter 5 a detailed analysis shall be performed into the origin and relationship between these defect bands.

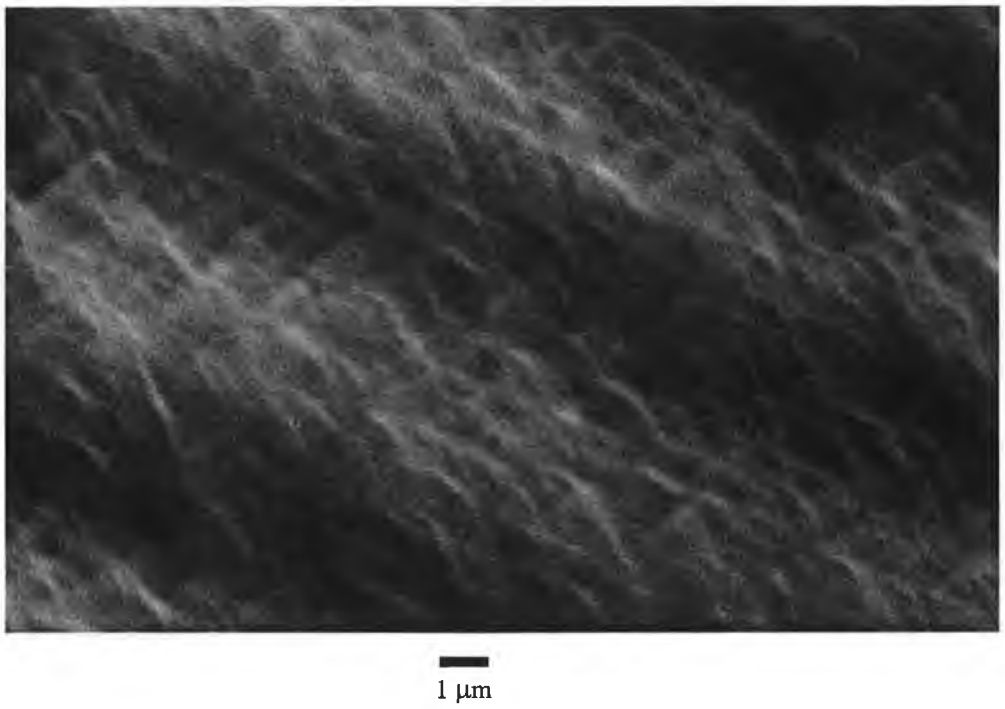

Figure 4.14: High resolution panchromatic cathodoluminescence image taken at 20 K, showing the light propagating from the crystallites in the ELO region

Figure 4.14 shows a high resolution panchromatic image of an ELO sample taken at 20 K. The non-ELO region is black, illustrating the poor luminescence efficiency of this material. Interestingly, from the ELO region, the light can be clearly seen originating from the hexagonal crystallites.

4.4 Getting the most from cathodoluminescence

In order to get the best out of cathodoluminescence a number of preparation techniques should be adhered to. While it is generally a simple technique, certain procedures should be taken to obtain satisfactory results. A short description will now summarize these conditions.

Firstly, samples should be cleaned before examination. This is best done placing the sample in a little acetone and placing it in an ultrasonic bath for about 15 minutes. It is best to dry the sample by waving it under some Nitrogen gas rather than wiping it dry. If the sample becomes contaminated it can severely hamper results. For instance figure 4.15 (a) shows a secondary electron image of an ELO sample that had not been cleaned prior to investigation. The sample contains a number of dust particles as shown. Figure 4.15 (b) shows a cathodoluminescence image from the same region as figure 4.15 (a).

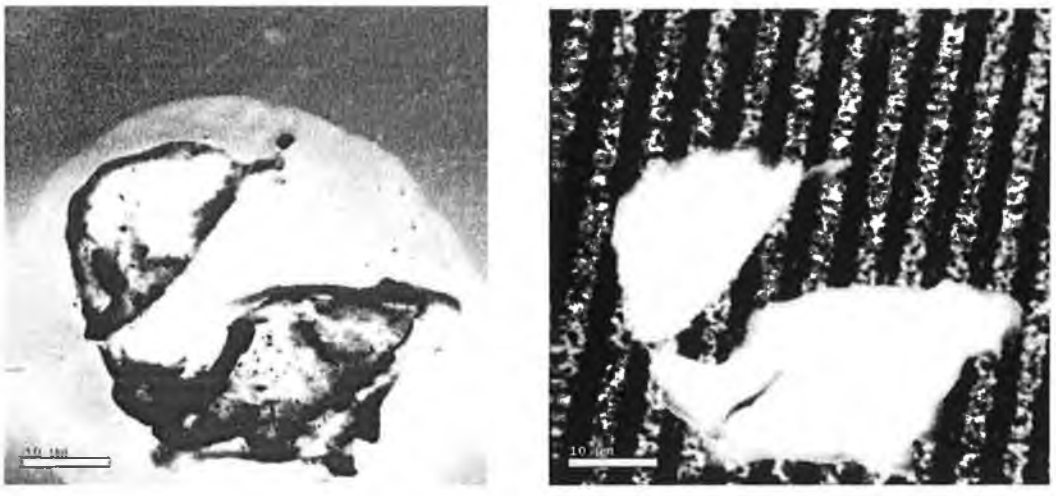

Figure 4.15: (a) Secondary electron image of contaminated region of ELO sample and (b) cathodoluminescence image of the same region

As can be clearly seen the dust/dirt particles block the luminescence escaping from the material and severely hampers the quality and information available from the final image.

Another issue that deserves attention is the alignment of the sample under the parabolic mirror. This can be a long, slow process, depending on the sample size and shape, but it deserves the utmost attention. The focal length of the mirror is 1 mm. This means that the sample to mirror distance should be exactly 1 mm. If this is not the case then the resulting CL image will be out of focus. There is also the danger of the sample colliding with the mirror rendering it useless if the sample stage is raised inside the 1 mm focal length. On the other hand much of the luminescence emitted from the sample will not be collected if the sample to mirror distance is greater than 1 mm.

Semiconductors when studied with the SEM are often the subject of a certain amount of charging. This can also hamper the quality of the secondary electron and cathodoluminescence images as shown in figure 4.16.

Figure 4.16: Secondary electron image of ELO material, showing charged region due to high probe current

This inner image was taken using a probe current of 10 nA and at a magnification of 10, 000 X. The beam was scanned across this region for 5 seconds. The magnification was then reduced to show the region originally exposed. The originally exposed region has charged and appears black. This can damage the sample and severely hamper the secondary electron or cathodoluminescence image.

Charging however may be reduced substantially by using lower probe currents, often less that 1 nA can suffice for SEM and CL investigations, however this issue is sample dependent. Also some silver conductive paint may be placed on the back of the sample to help conduct the electrons and substantially reduce charging effects.

5 Photoluminescence results

5.1 Introduction to metastability

Metastable defects in compound semiconductors such as GaN have recently been the subject of much interest. Metastability is a property inherent to all defects characterised by a non negligible electron phonon interaction. This interaction induces a relaxation or distortion of the lattice atoms surrounding the defect. In this case the electronic transitions between the defect and the band can be modelled using a configuration coordinate diagram such as that in figure 1.6.

However in many cases metastability is only characterised by the well known persistent photoconductivity (PPC) effect [Bourgoin 2000] which has been observed by many groups in the case of GaN [Chen *et al.* 1997], [Hirsch *et al.* 1997], [Beadie *et al.* 1997].

A particular defect, with a non negligible electron phonon interaction, has a ground state of atomic configuration A. When the semiconductor is illuminated by the laser its charge state may change and the initial electron phonon interaction is modified. This modification induces a change in the atomic configuration. If the modification is so large that it results in a totally different atomic configuration, the defect is said to be bistable, since it exhibits two different atomic configurations for two different charge states.

The metastable defect is however different in that the atomic configuration is different from the original, but the charge state remains unchanged [Bourgoin 2000]. The figure below shows a configuration coordinate diagram for both the bistable and metastable states.

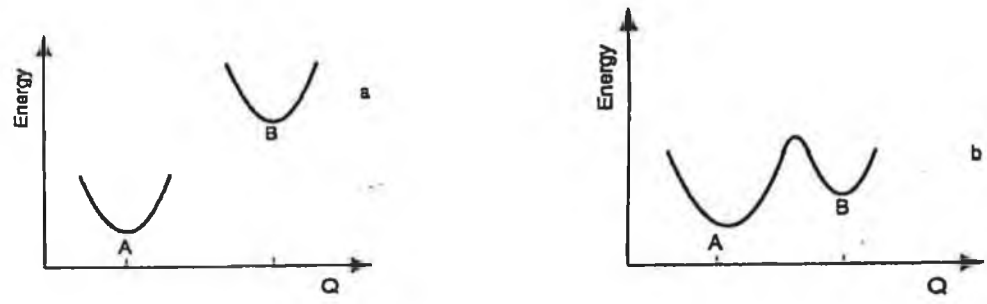

Figure 5.1: Configuration coordinate diagram of (a) bistable and (b) metastable state

5.2 Models for metastability

An interesting model for metastability discussed by Bourgoin [Bourgoin 2000] shall now be described. An electron occupying the ground state E_g of an atomic configuration g is characterised by some distortion induced by the electron phonon interaction. Under photo excitation the electron is transferred to an excited state and the original ground state electron phonon interaction disappears. As a result the atomic configuration changes. The new configuration e possesses a new ground state E_e see figure 5.2 (a).

The electron is initially trapped on one of the excited states of the e configuration. This decay via phonon emission from one excited state to a lower energy state occurs to the ground state E_e. This decay process cannot proceed to E_g since the corresponding atomic configuration for this state no longer exists. In order for the electron localised on E_e to get trapped on the original configuration E_g the temperature must be high enough for the original state to be restored as in figure 5 (b). That is the phonon energy must be larger than the barrier for electron capture B in order to induce the change form the e to the g configuration. Therefore the e configuration is metastable. Hence all deep level defects characterised by a non negligible electron phonon interaction possess a potential metastable state. In order to observe such a state the following conditions must be met:

- Temperature must be low enough so that the e configuration exists

- The E_e state must be filled – temperature low enough so that $kT < B$
- Metastable state must be filled before transforming to the stable state - $E_e > B$

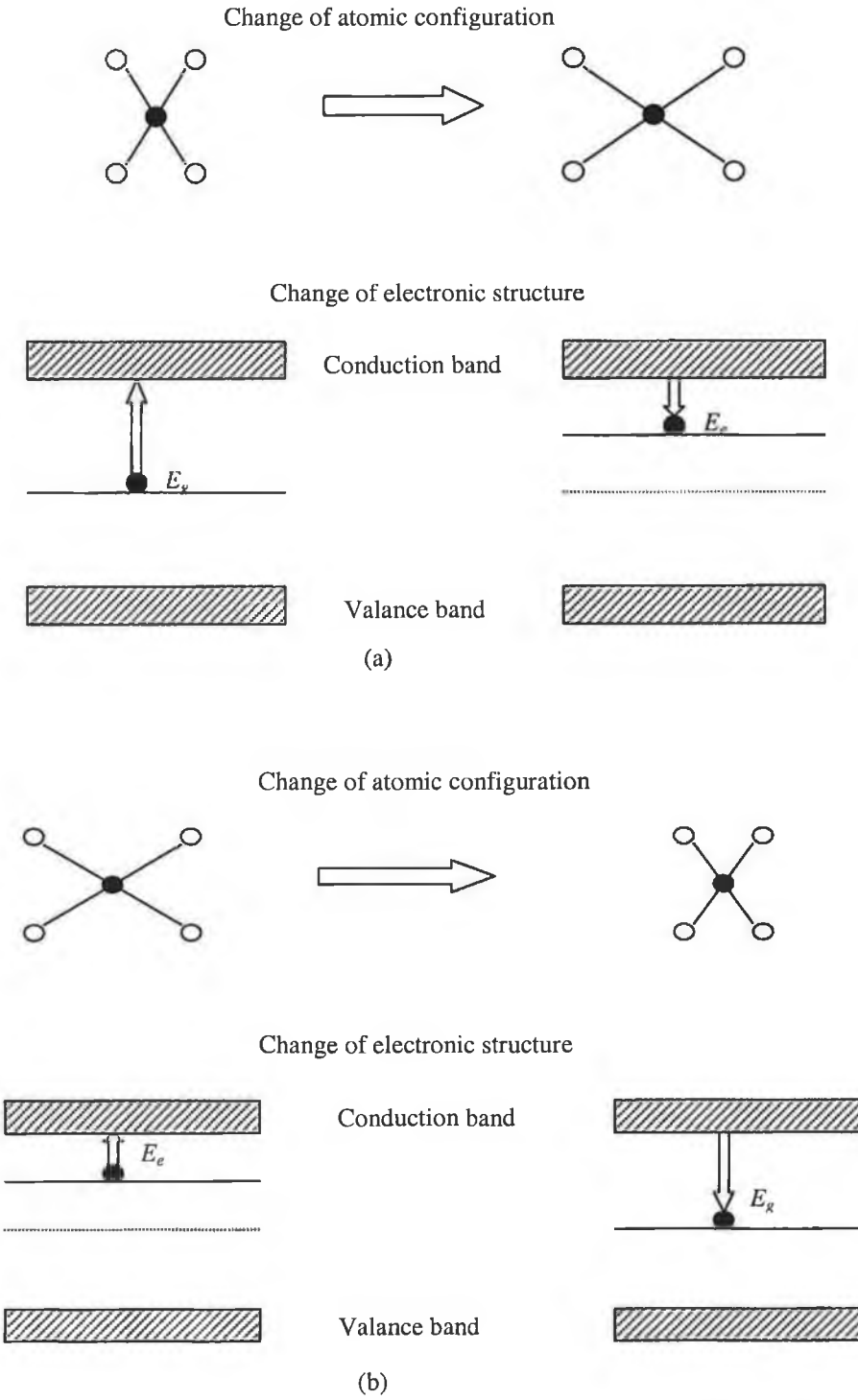

Figure 5.2: (a) Illustration of change of atomic configuration of a defect due to photo excitation and corresponding change of electronic structure. The change in electronic structure sees the E_g state disappear. The electron as a result recombines on the ground state of E_e. This constitutes the metastable state. (b) When the temperature is increased the original configuration is restored by atomic vibrations. The original ground state reappears allowing electrons to occupy it. This induces the transition from the metastable to the normal state.

5.3 Metastable 2.9 eV luminescence band in GaN

The blue luminescence band centred at ~ 2.9 eV, which appears in certain samples and fatigues under illumination has been attributed to a metastable defect [Xu *et al.* 1998]. Supporting evidence comes from long lifetime persistent photoconductivity (PPC), which persists for over 150 minutes after the light source is removed [Chen *et al.* 1997].

The 2.9 eV origin is however unclear but strong evidence exists for the donor acceptor pair model [Gruzintsev *et al.* 2001], [Reshchikov *et al.* 2000]. Toth *et al.* suggest the involvement of O_N and hydrogenated Ga vacancies [Toth *et al.* 1999], while Kaufmann suggest a deep donor, attributed to a nearest neighbour associate of a Mg_{Ga} acceptor with a N vacancy [Kaufmann *et* al. 1998].

In this study, we explore the temperature dependence of the changes that take place in the 2.2 and 2.9 eV intensities for both constant illumination and intermittent illumination over longer time scales than previously researched.

5.4 Experimental description

The experiment was performed using the Fourier Transform spectrometer apparatus described in section 3.1.2. The laser intensity used was ~ 0.65 W/cm^2. The sample was cooled in the dark with the laser off to the required temperature. Spectra were obtained within seconds of switching on the laser. Both constant and intermittent illumination measurements were performed. In the case of constant illumination the sample was exposed to the laser for a continuous three hour period and spectra were obtained every few minutes.

For our intermittent study the sample was exposed to the laser and a spectrum was obtained. The laser was then immediately switched off for a period of ~ 30 minutes and then switched back on in order to obtain another spectrum. This study was performed to examine the effect of the thermal destruction of the 2.9 eV band and was performed for the same exposure time as the constant illumination study.

The sample investigated was a 2 μm thick undoped GaN epilayer grown directly on a c-plane sapphire substrate of thickness 430 μm using MOCVD. This sample was supplied by Emcore.

5.5 Results

Figure 5.3 shows representative low resolution PL spectra recorded at a number of temperatures. The bandedge (BE) emission appears as a single weak peak at ~ 364 nm, while the 2.9 and 2.2 eV bands are both rather broad. The bands are sufficiently well separated to enable the changes in the band intensities to be observed and measured. The PL spectrum below is strikingly different from CL spectrum from the sample in figure 4.12. This may be due to the different excitation mechanisms i.e. excitation from a focussed electron beam, and excitation from an unfocussed UV laser beam. Also researchers have shown vastly different spectra for different GaN samples [Shalish *et al.* 1999]

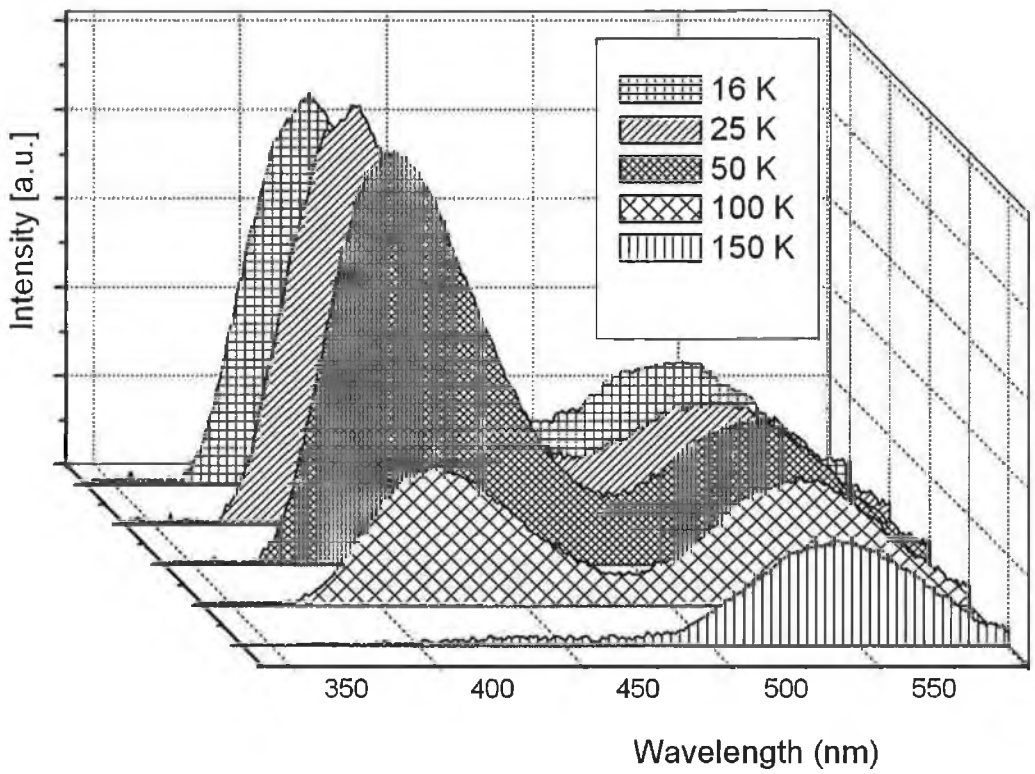

Figure 5.3: PL spectra taken at various temperatures

The spectra display the typical temperature dependence of the bands, with the 2.9 eV band getting weaker as the temperature is increased and finally vanishing at relatively low temperatures (~ 150 K). We report on how the intensities of these bands change with time at various temperatures and for both constant and intermittent illumination. Photoluminescence spectra recorded for constant illumination at 16 K over a period of 3 hours are shown in Figure 5.4.

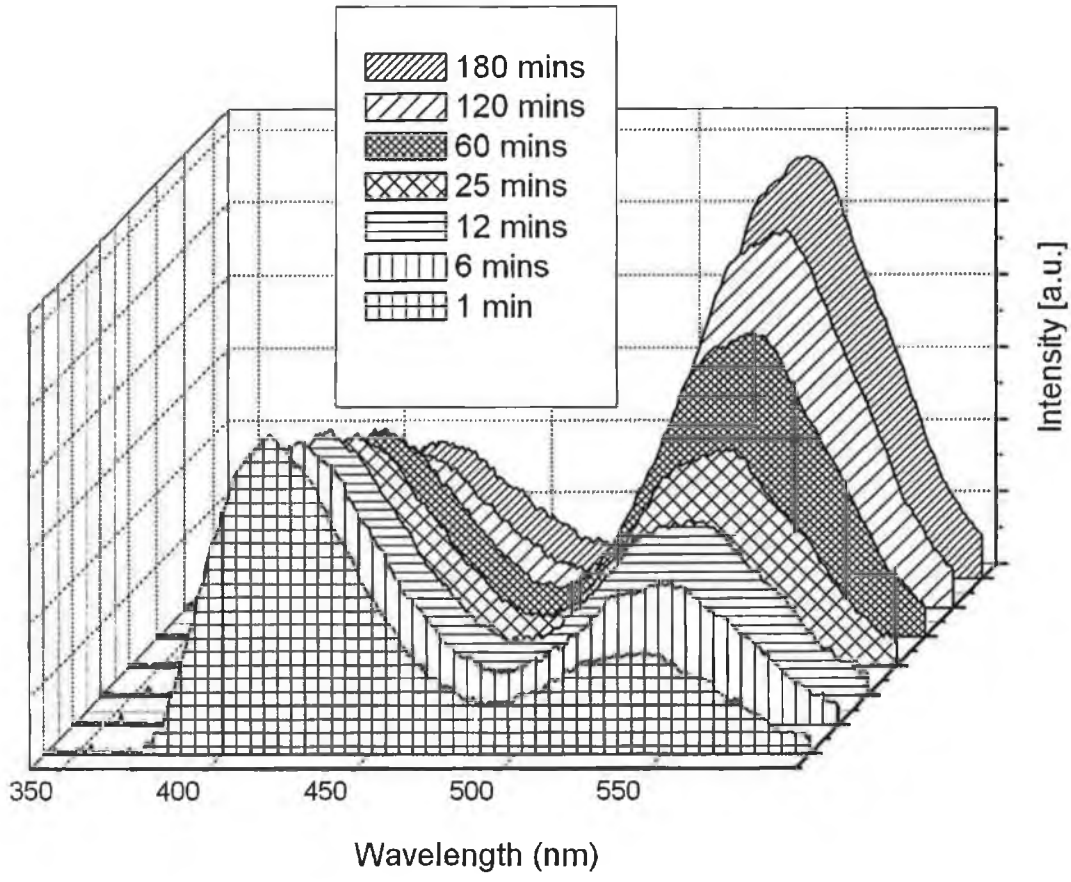

Figure 5.4: PL spectra at intervals over three hour exposure at 16 K

The sample glows bright blue upon initial exposure to the laser and gradually changes to yellow over time. Similar effects are observed for other temperatures and the complete set of results is presented graphically in Figure 5.5 (a) and (b).

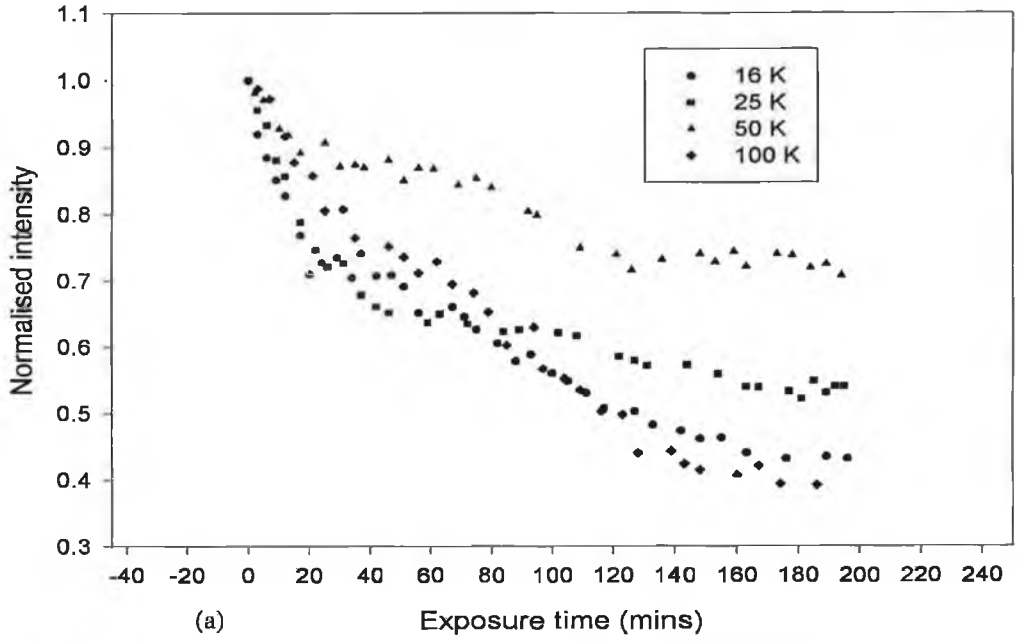

(a)

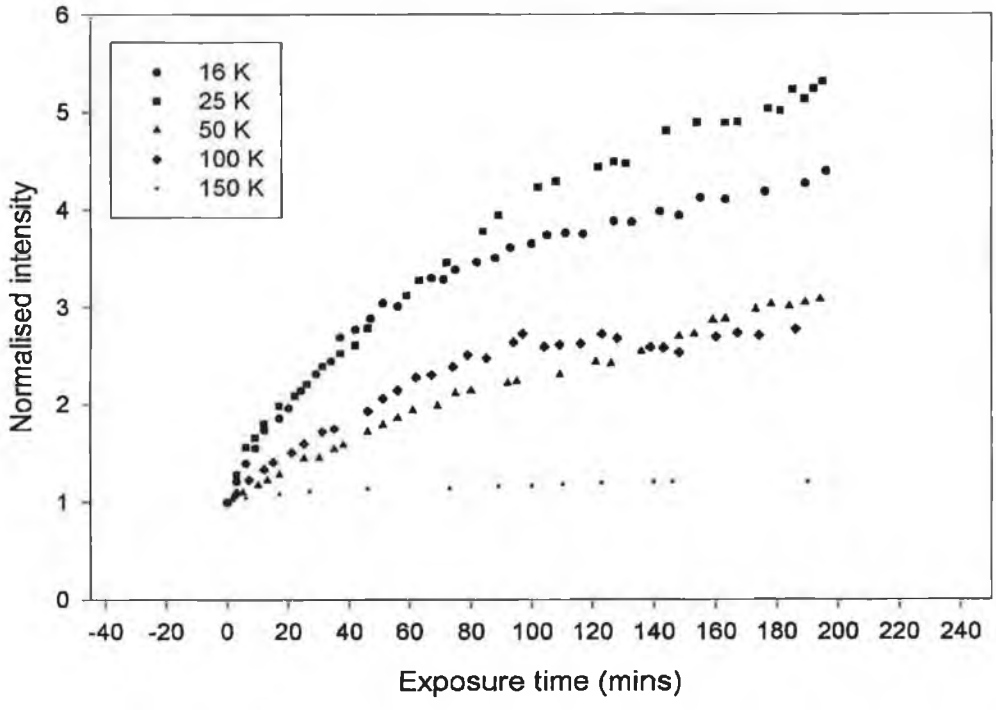

(b)

Figure 5.5: (a) Rate of decrease of 2.9 and (b) increase of 2.2 eV luminescence band with exposure time as a function of temperature

The decay of the 2.9 eV intensity is characterised by a relatively fast initial decay followed by a slower process for longer times, with the latter being noticeably temperature dependent. The data for 16 K and 25 K have been fitted to a double exponential decay of the form $y = a*\exp\left(-t/\tau_1\right) + c*\exp\left(-t/\tau_2\right)$, and the values obtained from the fits are listed in table 5.1. For the higher temperatures, a single decay fit of the form $y = y_0 + a*\exp\left(-t/\tau\right)$ was sufficient. In a similar fashion, we obtained the characteristic times for the concurrent growth in the 2.2 eV intensity. For these data, a single growth process plotted to $y = y_0 + a*\left(1-\exp\left(-t/\tau\right)\right)$ provides good fits.

Temperature K	Blue band decay τ_b (mins)	Yellow band growth τ_y (mins)
16	$\tau_{b1} = 6.9$ $\tau_{b2} = 277$	61
25	$\tau_{b1} = 17$ $\tau_{b2} = 769$	112
50	$\tau_b = 115$	222
100	$\tau_b = 152$	52
150	-	50

Table 5.1: Characteristic times of 2.9 and 2.2 eV changes at a range of temperatures

For all cases, the τ values have considerable uncertainties, and they should be viewed as indicative of the general behaviour of the bands rather than as definitive values. Figure 5.5 (a) shows that the intensity of the residual 2.9 eV luminescence that persists after prolonged irradiation increases with temperature up to 50 K. This raises the question of whether the 2.9 eV band consists of two or more overlapping bands with different temperature and fatigue characteristics.

It was also noted that the growth rate of the 2.2 eV band does not have the same characteristic timescale as the decay of the 2.9 eV band and so we can rule out a direct connection between the defects responsible for these two bands.

The photoluminescence intensities at a particular temperature are influenced not only by the illumination but also by the duration of storage at that temperature, i.e. there are both thermal annealing and optical effects at play. We explore this issue by illuminating the sample for only as long as is required to record the PL spectrum, then shutting off the illumination for a period. This was performed for a period of up to three hours. Only a minor effect was observed for T = 16 K, with a drop of less than 10% in the 2.9 eV intensity. Increasing the temperature has a significant effect however.

Figure 5.6 shows the results obtained for 25 K.

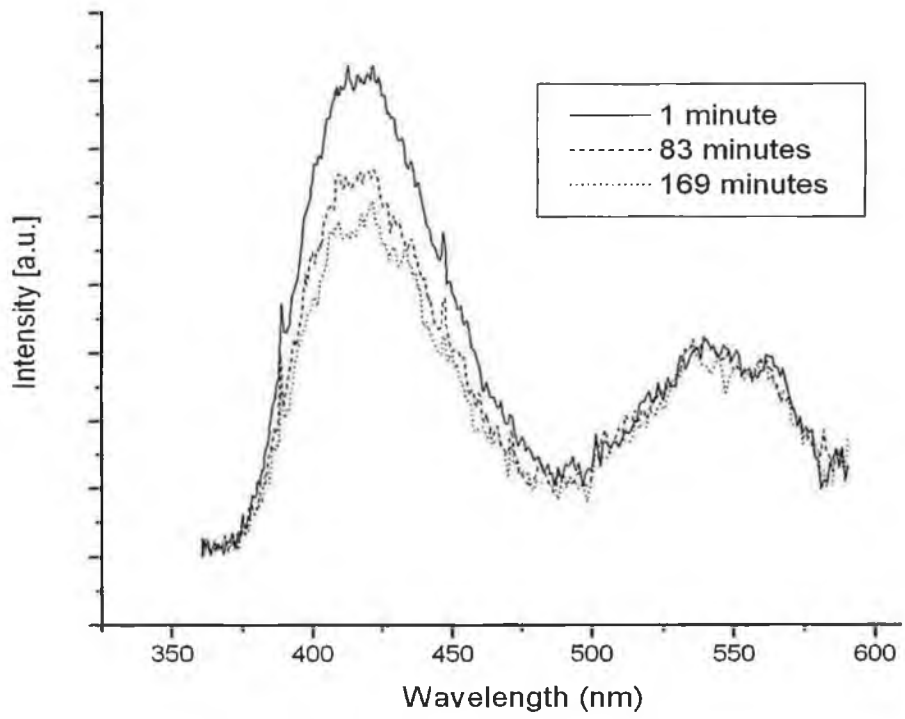

Figure 5.6: Intermittent measurements at 25 K

After almost three hours, the 2.9 eV intensity falls by about 25 % of its initial value. The most notable difference from the case of constant illumination is that there is no change in the 2.2 eV intensity. This effect for intermittent illumination – a loss of 2.9 eV intensity without affecting the 2.2 eV intensity – occurs also for higher temperatures. The intermittent illumination effects are quite complex, however, as

becomes evident from studying the trends for different temperatures. Data for 16 and 25 K are presented in Figure 5.7.

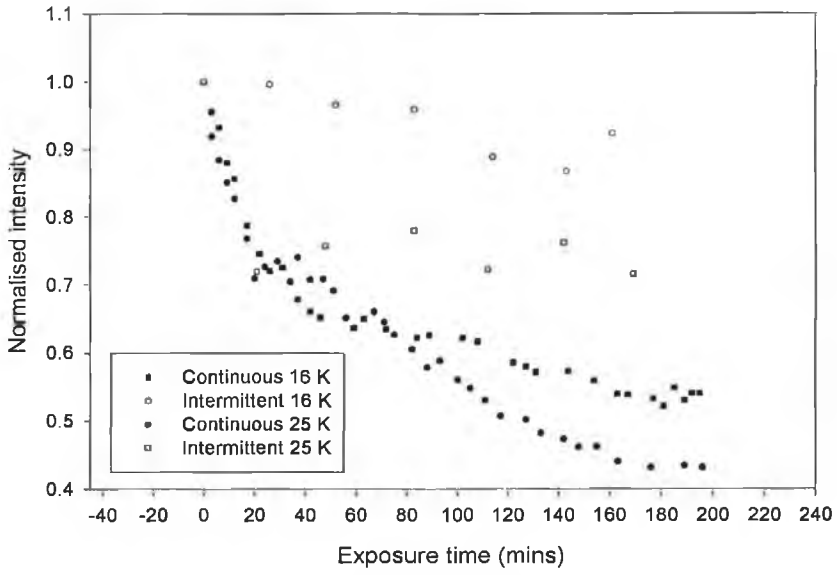

Figure 5.7: Fatigue nature of the blue band under constant and intermittent illumination

For all except 16 K, there is an initial a fast decay process for which the rate of decrease corresponds to that observed for constant illumination, i.e. over the first 30 minutes or so there is no difference between constant and intermittent illumination. For longer times, the presence or absence of illumination makes a considerable difference at temperatures above 16 K. A common factor is the absence of the slow decay process observed under constant illumination. Another common factor is the result that the stable component of the 2.9 e V intensity for intermittent illumination is approximately 75% of the initial intensity.

5.6 Discussion

The data we have obtained correspond broadly to the reported data for times up to about 50 minutes [Xu *et al.* 1998, Kim *et al.* 1999]. While we have not recorded the rapid changes which take place over the first three or four minutes [Xu *et al.* 1998, Kim *et al.* 1999], by extending the study to longer times we show an additional long tail on the bleaching of the 2.9 eV and growth of the 2.2 eV bands not reported in earlier studies. Significantly, we show that the bleaching is noticeably different for conditions of brief illumination in comparison to constant exposure to the laser. We

note that the normalised 2.9 eV intensity (Figure 5.5 (a)) for longer exposure times under constant illumination increases with temperature for 16 – 50 K, and then falls again by 100 K. We infer the following from these results.

The 2.9 eV luminescence in the sample studied here consists of at least two overlapping bands as discussed in [Gruzintsev *et al.* 2001]. The defects producing one of these bands are unstable at temperatures in the region of 25 K and upwards, resulting in the loss of about 25 % of the BB intensity after times of 30 minutes or less, with or without exposure. The loss of this luminescence does not lead to a change in the 2.2 eV intensity. The remainder of the 2.9 eV luminescence is due to defects which are unstable under irradiation at all temperatures. The bleaching rate and the luminescence intensity for these defects are both temperature dependent, which results in the complex data displayed in Figure 5.5 (a). The loss of this luminescence does lead (indirectly) to an increase in the 2.2 eV intensity. This suggests that there is competition between two opposing processes for this part of the 2.9 eV luminescence. One the one hand, illumination tends to destroy the defects, causing a slow decrease in the 2.9 eV intensity over time. On the other hand, increasing the temperature creates a reverse process which tends to oppose this bleaching. We would expect this to lead to a slower decay rate of the 2.9 eV intensity at higher temperatures, which we observe up to 50 K. By 100 K, the 2.9 eV luminescence is becoming thermally deactivated, and the overall BB intensity decreases markedly and the bleaching process gets faster.

There are various candidate identifications for the 2.9 eV luminescence, mostly involving donor-acceptor (DA) recombination [Reshchikov *et al.* 2000, Toth *et al.* 1999, Kaufmann *et al.* 1998], but we are not in a position to decide this question from the available data. The excitation density used (approximately 0.65 W/cm^2) is sufficiently high to saturate DA recombination if the acceptor concentration is low, as we would expect for our n-type material. Accordingly, it is possible that we have some acceptors with two captured holes under illumination. The bleaching of such defects would be a two-stage process, requiring sequential capture of two electrons. This could help explain the complex decay patterns, including the temperature

effects, since the barriers to electron capture will change depending on the charge state of the acceptor defect.

Lastly, in the case for the 2.9 eV band, we have found that applying the stretched exponential analysis [Chen *et al.* 1992, Pavesi *et al.* 1993] based on the equation $I = I_0 \exp\left(-t/\tau\right)^{\beta}$ is unsuccessful for our full data set. This equation assumes that a spread of τ values applies to the transient process with β, the dispersion factor, giving a measure of the spread in τ. We conclude that the bleaching processes active in our sample do not involve a simple carrier diffusion process for which the stretched exponential model is valid.

Our results for the 2.2 eV luminescence band indicate no direct connection between the bands. Firstly, the loss of 2.9 eV intensity does not necessarily lead to greater 2.2 eV intensity, and the rate of growth of the latter does not correspond always to the rate of decay of the former. We support the view that changes in 2.2 eV intensity are a consequence of the removal of competing luminescence channels rather than of a simple direct conversion between two configurations of one defect.

6 Conclusions and suggestions for future work

This characterisation study of GaN firstly presents an interesting comparison between non-ELO material and ELO grown material at both room temperature and low temperature. Strong defect bands were observed in non-ELO material and this behaviour is thought to be due to its poor structural quality. However it highlights some problems that require attention, such as the exact origin of the blue and yellow bands and the possible relationships between them.

It was demonstrated also how powerful a technique cathodoluminescence can be to the study of semiconductors from both a spectra and imaging viewpoint and outlines some careful considerations which must be taken to ensure optimum performance.

The scope for further work using cathodoluminescence is quite extensive. Many other important wide bandgap materials such as ZnO can be examined for their luminescence quality. Cathodoluminescence has applications not only restricted to semiconductors but also in the field of geology, diamond materials and ceramic [Heard 1996]. Many research groups are combining cathodoluminescence imaging also with Electron Dispersive Spectroscopy (EDS). This allows a researcher the luxury of having spectroscopy, compositional information and imaging all in one system.

The defect bands observed from the ELO study lead our work to a recent popular area of GaN research. That is the origin of the 2.9 eV luminescence band and its possible interrelationship with the 2.2 eV luminescence band. In the past three years research groups have started to study this interesting phenomenon [Reshchikov *et al.* 2000, Dhar *et al.* 2002]. Our work has dealt with some of the very complex theoretical aspects of metastability as well as presenting some of the experimental results. This area of GaN research is very new and therefore plenty of scope exists for new results and theories. The phenomenon is very much sample dependent as other samples were tried and didn't show any sign of photoinduced changes.

There is much scope for future work in this field. A starting point for this is using a variety of well characterised samples in order to get a more general overall picture of how the process varies from sample to sample.

7 References

Akasaki I. *et al.* J. Lumin. 40-41 121 1988

Amokrane A. *et al.* J. Phys: Condensed Matter 12 10271 – 10278 2000.

Beadie *et al.* Appl. Phys. Lett. 71 (8) 1092-1094 1997

Bell A. *et al.* International Conference for the Physics of Semiconductors (ICPS) 2001.

Bhattacharya P. K. Semiconductor optoelectronic devices, Prentice-Hall international, London, 1994.

Blakemore J. S. Solid state physics - 2nd ed. – Cambridge [Cambridgeshire]; New York : Cambridge University Press, 1985.

Bourgoin J.C. Solid State Phenomena 71 73-92 2000

Brandon D. & Kaplan W. D. Microstructural characterisation of materials, Chichester: Wiley, 1999.

Brown S.A. *et al.* Appl. Phys. Lett. 75 (21) 3285-3287 1999.

Chamberlain J. E. The principles of Interferometric spectroscopy Chichester; New York: Willey 1979.

Chen H. M. *et al.* J. Appl. Phys. 82 (2) 899-901 1997

Chen X. *et al.* Appl. Phys. Lett. 60 (21) 2672-2674 1992

Dhar S. *et al.* Appl. Phys. Lett. 80 (24) 4519 – 4521 2002.

Drouin D. *et al.* monte CArlo SImulation of electroN trajectory in sOlids CASINO

software 1997. – Download from: http://www.gel.usherb.ca/casino/

Eisberg R. M. & Resnick R. - Quantum physics of atoms, molecules, solids, nuclei, and particles - 2nd ed. - New York: Wiley, 1985.

Fox M.A. Optical Properties of Solids: Oxford University Press Inc., 2003

Gatan UK, MonoCL3 with DigiScan Operators handbook, Issue 1, January 2001.

Glaser E.R. *et al.* Phys. Rev. B 51 13326 1995.

Godlewski M. *et al.* J. Luminescence 87-89 1155-1157 2000.

Gruzintsev A.N. *et al.* Inorganic materials 37 (6) 591-594 2001.

Heard P. Microscopy and Analysis 1996

Henry M.O. *et al.* To be published in Physica B

Hersee S. D. *et al.* MRS Bull 22 (7) 44-51 1997.

Hirsch M.T. *et al.* Appl. Phys. Lett. 71 (8) 1098-1100 1997

Hoff P. H. *et al.* J. Appl. Phys. 42 (13) 5837-5846 1971.

Hummel R. E. Electronic properties of materials. - 3rd ed. - London; New York, NY : Springer, 2001.

Jain S. C. *et al.* J. App. Phys, 87 (3) 965-1006 2000.

JEOL – A guide to scanning electron microscopy – Download from: http://www.jeol.com/sem_gde/guide.pdf

Johnson M.A.L. *et al.* Journal of Electronic Materials 28 (3) 1999.

Kanaya K. & Okayama S. J. Phys. D: Appl. Phys. 5 43-58 1972.

Kaufmann U. *et al.* Appl. Phys. Lett. 72 (11) 1326-1328 1998

Kim B. *et al.* J. Appl. Phys. 86 (4) 2034-2037 1999.

Klein C. A. J. Appl. Phys. 39 2029 1968

Koleske D. D. *et al.* DARPA meta-materials workshop, Sept 2000.

Mah K.W. *et al.* Journal of Crystal Growth 222 (3) 497-502 2001

Matsuoka T. GaN and Related Materials (Edited by S.J. Pearton) Gordon and Breach Science Publishers 1997

Mattila T. *et al.* Phys. Rev. B 55 9571 1997.

McNally P.J. *et al.* Phys. Stat. Sol. (a) 185 (2) 373-382 2001.

Nakamura S. *et al.* Appl. Phys. Lett. 72 (2) 211-213 1998.

Nakamura S. *et al.* Jpn. J. Appl. Phys. 31 L139 1992

Ogino T. *et al.* Jpn. J. Appl. Phys. 19 2395 1980.

Omar A. Elementary solid state physics: principles and applications, Reading, Mass: Addison-Wesley Pub. Co, 1975.

Orton J. W. & Foxon C. T. Rep. Prog. Phys. 61 (1) 1-75 1998.

Palmer C. Diffraction grating handbook - 4th ed. – Richardson grating laboratory 2000.

Pankove J. I. Optical processes in semiconductors, Dover pub. Inc., New York, 1971.

Pankove J.I. Material Science and Engineering B61-62 305-309 1999

Pavesi *et al.* Phys Rev. B 48 (23) 17625-17628 1993

Perkowitz S. Optical characterization of semiconductors, Academic Press: London, San Diego, 1993.

Petrov, V. I. Physics-Uspekhi 39 (8) 807-818 1996.

Ponce F.A. *et al.* Appl. Phys. Lett 68 (1) 57-59 1996

Reshchikov M. A. *et al.* Physica B (273 – 274) 105 – 108 1999.

Reshchikov M.A. *et al.* J. Appl. Phys. 87 (7) 3351-3354 2000

Rudden M. N. & Wilson J., Elements of solid state physics, - 2nd ed. – Chichester [England]; New York: Wiley, 1993.

Seifert W. *et al.* Cryst. Res. Technol. 18 383 1983

Shahedipour F. J. *et al.* Appl. Phys. 87 (7) 3351-3354 2000.

Shalish I. *et al.* Phys. Rev. B 59 (15) 9748 – 9751 1999.

Stoneham A. M. Theory of defects in solids, Clarendon Press, Oxford, 1975.

Toth *et al.* Phys. Rev. B 59 (3) 1575-1578 1999

Van Veckten *et al.* J. Appl. Phys. 31 3662 1992

Varshni Y.P. Physica 34 149 1967.

Xu S.J. *et al.* Appl. Phys. Lett. 72 (19) 2451- 2453 1998.

Yacobi B. & Holt D. Cathodoluminescence microscopy of inorganic solids, Plenum Press, New York 1990.

Yu Z. *et al.* MRS Internet J. Nitride Semicond. Res. 3 6 1998.